Spatial variability of liquid water path in marine low cloud: Part II. Geographic distribution and dependence upon large-scale parameters.

ROBERT WOOD* and DENNIS. L. HARTMANN

University of Washington, Seattle, Washington

October 6, 2004

Corresponding author address: Dr. Robert Wood, Atmospheric Sciences, University of Washington, Seattle, WA; *e-mail: robwood@atmos.washington.edu.*

Abstract

In part I of this study we focused upon models to describe the mesoscale spatial variability of cloud liquid water path LWP in low cloud. Here, we construct simple, exploratory, climatologies of the spatial variability characteristics of marine low clouds for one season and two regions of the East Pacific. The climatologies show interesting and important geographical variability. Large scale meteorological conditions are assessed for each MODIS scene using NCEP/NCAR reanalysis data, and regression analysis is used to assess relationships between large-scale forcings and mesoscale variability. Cloud fraction and LWP homogeneity are both strongly correlated with lower tropospheric stability LTS on timescales of days to weeks. While marine boundary layer (MBL) depth z_i is itself strongly correlated with LTS, cloud fraction is not found to correlate particularly well with z_i, suggesting that it is LTS itself, rather than z_i that is the primary determinant of low cloud fraction. However, MBL thermodynamic and cloud mesoscale variability does appear to be influenced by z_i. This result reflects the findings that mesoscale variability is an increasing function of the characteristic lengthscale of the mesoscale cellular convection (MCC), and that the characteristic lengthscale scales with z_i. The observed changes in cloud mesoscale variability from shallow stratus-topped MBLs through to trade cumulus can be accounted for using a physical framework that links MBL thermodynamic variability and cloud liquid water path variability using a pdf formulation. The pdf width is strongly tied to the MBL depth, and it is suggested that this framework, with scalings constrained by observations, is suitable for the parameterization of low cloud subgrid spatial variability in large-scale numerical models.

1. Introduction

Spatial variability in marine boundary layer (MBL) low cloud is ubiquitous and is important both radiatively and dynamically (Cahalan et al. 1994; Rossow et al. 2002; Pincus and Klein 2000; Rotstayn 2000; Larson et al. 2001; Wood et al. 2002). Despite this importance, so far only limited attempts have been made to systematically quantify this variability over large regions of the oceans on timescales appropriate to large-scale numerical modeling, and the attempts that have been made tend to aggregate the effects of all cloud types (e.g. Rossow et al. 2002).

In Part I of this study we presented a method to break Moderate Resolution Imaging Spectroradiometer (MODIS) liquid water path data into 256×256 km "scenes" to which we then apply a number of analysis tools including probability density function (pdf) and power spectral analysis. We found that three variables (mean cloud-only liquid water path $\overline{LWP}$, cloud fraction CF, and the square of the ratio of the mean to standard deviation of cloud-only liquid water path γ_{LWP} provide a fairly complete description of the one point LWP statistics in MBL clouds. We also found that a simple Gaussian model of the saturation excess pdf (or, equivalently $z_i - LCL$ pdf, where LCL is the local lifting condensation level) is quite successful at modeling the relationship between CF and cloud liquid water path variability. This model ties together the thermodynamic and cloud structure of the MBL in a way that may be suitable for parameterization in large-scale numerical models (see e.g. Park et al. 2004, which adopts an identical pdf form).

In Part II of this study, we continue our investigation into spatial variability in marine low cloud. We focus here upon simple climatologies of the spatial variability characteristics for two regions of the East Pacific Ocean (see Part I for details of the regions studied). In addition, we extend our analysis using data from the NCEP/NCAR reanalysis to assess relationships between

mesoscale spatial variability and associated large-scale forcings. We also examine a scaling between mesoscale cellular convection (MCC), spatial variability and MBL depth which may prove to be useful in the parameterization of mesoscale spatial variability and CF in MBL clouds.

2. Datasets used

Data used in this study are detailed in Part I, and only a brief description is given here. We use 1 km (at nadir) pixel data from the Moderate Resolution Imaging Spectroradiometer (MODIS) on the NASA Terra polar-orbiting sun-synchronous satellite. We estimate liquid water path LWP from the optical thickness and effective radius estimates in the Level 2 cloud product, and this is the primary dataset analyzed. Only daytime ($\sim$ 10:30 LST) scenes containing exclusively warm cloud are analyzed. All available MODIS data from September and October 2000 are used.

Reanalysis data from NCEP/NCAR (Kistler et al. 2001) are used to investigate links between large-scale meteorology and mesoscale spatial variability. Our methodology is to obtain a set of pertinent reanalysis variables for each of the MODIS scenes analyzed. Reanalysis data are available four times daily on a 2.5$\times$2.5° grid, and include sea surface temperature data (Reynolds and Smith 1994). Trilinear interpolation is used to determine the values of the reanalysis variables at the MODIS scene-center locations and times. We consider three large-scale variables derived from reanalysis in this study: lower tropospheric stability ($LTS = \theta_{700} - \theta_0$, where θ_{700} and θ_0 are the potential temperatures at 700 hPa and the surface respectively); large-scale vertical motion at 850 hPa (w_{850}); surface temperature advection $\mathbf{U} \cdot \nabla SST$, where $\mathbf{U}$ is the surface wind and SST is the sea surface temperature. Because it is known that there exists a sizeable diurnal cycle in surface divergence and subsidence rates above the MBL (Dai and Deser 1999), we use the mean w_{850} for the 24 hour period centered on the time of the MODIS overpass. This is unnecessary for

the other reanalysis parameters as their diurnal cycles are much weaker.

3. Geographic dependence of mesoscale variability

Two month means (September/October 2000) are used to show geographic dependence of the cloud mesoscale variability parameters. Data are binned into $2.5\times2.5^\circ$ boxes to produce maps. The number of MODIS scenes contributing to each $2.5\times2.5^\circ$ average for the two month period is between 10 and 60. The only boxes having less than 50 contributing scenes are either those very close to the coasts, and those where high cloud contamination is significant (see Fig. 1 in Part I of this study), specifically in the ITCZ (5-15°N), to the north of 40°N and to the south of 25°S.

a. LWP pdf parameters

Median values of $\overline{LWP}$ (mean LWP of cloudy fraction) range from around 40 g m^{-2} to 80 g m^{-2} (Fig. 1(a,b)). In the NE Pacific, $\overline{LWP}$ increases slightly, from around 40-50 g m^{-2} in the stratus regions near the Californian coast, to around 60 g m^{-2} in the trade wind regions. The trend is similar in the SE Pacific, with low values close to the Chilean coast, increasing downwind. However, $\overline{LWP}$ tends to decrease again in the SE Pacific trade winds. This weak variability in $\overline{LWP}$ is possibly indicative of important feedbacks discussed in Part I. A general feature (not shown) is that in regions with high climatological cloud fraction ($\overline{CF} > 0.6$), $\overline{LWP}$ is positively correlated with CF, whereas there is little correlation for regions where the mean CF is lower.

Maps of CF and γ_{LWP}[1] (Fig. 1) demonstrate the strong connection between these parameters examined in part I. The most homogeneous LWP (and the highest CF) is found along the Cali-

[1]Note that $\gamma_{LWP} = (\overline{LWP}/\sigma_{LWP})^2$ is the nondimensional homogeneity parameter introduced in Part I.

fornian and Chilean coasts, and decreases toward the remote ocean and trade-wind regions. The coverage of both unbroken (e.g. $CF > 0.6$) and homogeneous cloud (e.g. $\gamma_{LWP} > 2$) is more extensive in the SE than in the NE Pacific during this season. A longer dataset will be required to determine whether the $CF - \gamma_{LWP}$ links exist on seasonal timescales. The clouds remain unbroken and homogeneous into the SE Pacific tropical equatorial region, quite unlike the situation in the NE Pacific, reflecting the location of the ITCZ and associated strong southerly cross-equatorial flow. Stronger cold advection in the NE Pacific stratocumulus region most likely hastens the decoupling process and rate of MBL deepening by increasing surface fluxes. Figure 2 shows mean z_i and surface winds for September/October 2000. MBLs originating close to the Chilean coast deepen far less rapidly (in the Lagrangian sense) than comparable MBLs in the NE Pacific as they advect equatorward. Therefore, the effect of MBL deepening upon decoupling (Bretherton and Wyant 1997) may be of reduced importance in the SE Pacific. There is evidence that mean entrainment rates in the region of maximum cloud cover in the SE Pacific are lower than those in the corresponding region of the NE Pacific (Wood and Bretherton 2004) which would reduce the significance of MBL deepening there.

b. Characteristic lengthscale

Figure 3 shows maps of the median characteristic cell size λ_1. We only include scenes with $CF > 0.2$ because obtaining λ_1 from low CF scenes is more uncertain. The smallest cells (< 20 km) are found over the cold water close to the Oregon/Californian coast, with a strong oceanward gradient. Cell sizes reach a maximum of around 40-45 km as the subtropical airmass advects over warmer waters and the MBL deepens. SE Pacific values show a somewhat similar trend with the smallest

values associated with regions of climatologically shallow MBLs (see Fig. 2). As in the NE Pacific, cell sizes reach around 40-45 km in the trades. Links between cell size, thermodynamic variance and MBL depth are explored in Section 5.

c. Homogeneous, open or closed mesoscale cellular convection?

The geographic dependence of the prevalence of homogeneous cloud (no MCC), closed MCC, open MCC, and heterogeneous cloud without clear MCC, (Fig. 4) indicates that homogeneous clouds are rare apart from north of 40°N, along the Californian/Baha coastline, and close to the Chilean coasts, all regions with the shallowest MBLs (Fig. 2). Closed and open MCC is very common over much of the NE and SE Pacific but is relatively more common in the SE Pacific during this season. The pattern of closed MCC fraction resembles that of $\overline{z_i}$ with most closed MCC occurring where $\overline{z_i} < 1500$ m. Open MCC becomes prevalent over the warmer water trade-wind regions of the SE and NE Pacific, and to the north of the equatorial cold tongue. The diagnosis of open MCC also tends to include heterogeneous mesoscale rolls that seem to be peculiar to the region north of the equatorial cold tongue. It should be noted that it is perhaps inappropriate to classify these rolls as open MCC, but further subclassification of the groups was not attempted in this study. Heterogeneous scenes with no clear MCC are common over warmer waters, and in the NE Pacific in general, during this season. It will be interesting to examine the seasonality of these cloud types using an extended dataset.

The transition (in a Lagrangian sense) from homogeneous, through closed and then open MCC regions can be conceptualized as the stratocumulus to cumulus transition (SCT, Bretherton and Pincus 1995; Bretherton et al. 1999; de Roode and Duynkerke 1997), with the most homogeneous

clouds being stratus, the closed MCC being stratocumulus, and the open MCC being more cumuliform.

4. The influence of large-scale parameters

Klein (1997) demonstrates that both LTS and temperature advection (cold advection positive) are positively correlated with nighttime low cloud amount at ocean weather station November (30°N, 140°W) in the subtropics. Our data also support these general findings, although in this study we focus additionally on the large-scale influence upon spatial variability in low cloud fields, as quantified using $\overline{LWP}$, γ_{LWP} and the characteristic length scale λ_1.

a. Geographical variation of means of large-scale parameters

Geographical variations of the means of the large-scale parameters corresponding to the MODIS scenes are shown in Fig. 5. Subsidence is a typical feature of the MBL cloud cases throughout most of the NE and SE Pacific regions, but MBL clouds are also found in regions of large-scale ascent, most notably in the ITCZ regions at latitudes of 5-15°N. There also appears to be strongly reduced subsidence, and even ascent, close to the northern Chilean coast, which may be related to a mountain-influenced sea-breeze structure (Garreaud and Muñoz 2004), although it cannot be ruled out as an artifact of the reanalysis data upstream of strongly sloping terrain. Strong lower LTS prevails in the eastern Pacific regions, particularly over the coastal upwelling regions of the subtropics. Temperature advection is largely positive (i.e. cold advection) throughout the two regions, apart from very close to the northwestern United States coastline and along the equatorial cold tongue. Very strong cold advection is observed to the north of the cold tongue as cool air

flows northward over a strong gradient in sea surface temperature.

Geographical variations of the mean CF as a function of both LTS and MBL depth are examined on the longer two monthly timescale using the $2.5\times2.5^{\circ}$ means (Figure 6). We only include SE Pacific data south of the equator where the surface forcing is relatively weak. In addition, we should emphasize that the mean cloud amounts discussed here are the mean values for the daytime (10:30 am local time) MODIS overpasses. Given that diurnal maxima in CF and mean liquid water path occurs typically at 3-6 am (Rozendaal et al. 1995; Wood et al. 2002), the MODIS cloud amounts (measured $\sim$6 hours after the peak) are fairly representative of the diurnal mean cloud amount.

There is a tight correlation between mean LTS and CF (r=0.86 and 0.90 for the NE and SE Pacific subtropical regions) which holds through the entire range of mean cloud amounts observed ($\sim$0.2 to $\sim$0.9). This correlation, which has been explored in previous work (e.g. Slingo 1980, 1987; Klein and Hartmann 1993; Klein 1997) forms the basis for the parameterization of low cloud in a number of large-scale numerical models. Klein and Hartmann (1993) show that the relationship between LTS and CF is remarkably strong on seasonal timescales and over large regions. The least squares fit for our data is close to that found for the climatological mean cloud amounts for a number of regions (Klein and Hartmann 1993), although we find the sensitivity of the mean cloud amount to the LTS to be 20% greater. This may be because of the underestimation by ISCCP of extensive low cloud cover in the shallowest boundary layers where the cloud top temperature is close to that of the sea surface, but it may also be a consequence of the larger averaging regions used in Klein and Hartmann (1993). Correlations between mean CF and z_i are almost as high as for LTS (0.81 and 0.87 for the NE and SE Pacific respectively), suggesting that boundary layer depth, lower tropospheric stability, and cloud fraction are interrelated and

inseparable elements in determining climatological cloud amounts in the subtropics. This new evidence implicating boundary layer depth as a major controlling parameter may be useful in determining a physical mechanism to explain the strong link between LTS and CF.

Next, we explore the significance of the strong correlation (r=0.88 for both NE and SE Pacific, not shown) between the 2.5×2.5° mean values of LTS and z_i. A linear fit to the mean values for both regions combined yields

$$LTS = \theta_{700} - \theta_0 = 26.6 - 5.8 \times 10^{-3} z_i. \quad (1)$$

The free-tropospheric vertical potential stratification $\Gamma_{FT} = d\theta/dz$ is a function of the large scale tropical-subtropical meridional circulation and is typically in the range $\Gamma_{FT} = 5{-}6{\times}10^{-3}$ K m^{-1} throughout the subtropics and the clear regions of the tropics (Betts and Ridgway 1988). The fact that Γ_{FT} is close to $d(LTS)/dz_i$ means that the difference between the potential temperature of air just above the MBL and that at the surface $\Delta\theta = \theta(z_i^+) - \theta_0$ is more or less constant over a wide range of z_i. From (1), we estimate $\Delta\theta =$ 8-10 K. This value is in agreement with in-situ observations over a wide range of MBL depths collated by Kuo and Schubert (1988). A nearly constant value $\Delta\theta \approx 9$ K is required to close the local liquid static energy budget in the subtropical MBL (Betts 1989), which is not strongly dependent upon cloud fraction. Our result is therefore evidence that the subtropical MBL is in approximate equilibrium with the radiatively driven subsidenfor both academic and research facultyce field (Betts and Ridgway 1988; Betts 1989) which characterizes the descending branches of the large-scale meridional circulation. Evidence for this approximate equilibrium was also given in Wood and Bretherton (2004) who found that mean entrainment rates into the MBL do not exceed mean subsidence rates by more than 30% throughout much of the subtropical East Pacific. Reversing the argument, the near equilibrium nature of the

MBL suggests that z_i adjusts on timescales longer than the MBL adjustment timescale of 1-2 days (Schubert et al. 36) to reach the balance $LTS = \Delta\theta - \Gamma_{FT}(z_{700} - z_i)$ where z_{700} is the height of the 700 hPa pressure level ($\approx$ 3 km). Thus, on long timescales LTS can be essentially thought of as an indicator of MBL depth.

b. Regression maps of daily data

Maps showing the regression of cloud-mean liquid water path $\overline{LWP}$, CF, and homogeneity parameter γ_{LWP} onto large scale parameters are shown in Figs. 7 (w_{850}), 8 (LTS), and 9 (temperature advection). Regressions were performed by first averaging the data from all the MODIS scenes in a $5\times5^{\circ}$ resolution grid for each day to create a daily timeseries at each gridbox. Not all days at each location contain data but this is not important for regression analysis.

The cloud-mean LWP is influenced strongly by w_{850} only the NE Pacific stratocumulus region close to the Californian coast, with positive w_{850} anomalies (reduced subsidence) associated with increased $\overline{LWP}$. Little effect is observed elsewhere, except to the north of the equator the SE Pacific, where a similar correlation is found. Vertical wind is uncorrelated with cloud fraction everywhere, and only weakly correlated with γ_{LWP} off the Baha peninsula, where increased subsidence favors more homogeneous cloud.

LTS is found to be uncorrelated with $\overline{LWP}$ in the NE Pacific, and only for a small region of the SE Pacific. However, LTS is strongly correlated with CF in both the NE and SE Pacific subtropical regions, particularly those with large climatological cloud amount. The evidence in Fig. 8 suggests that in many areas this relationship exists on scales of days to weeks, and on quite small geographical scales. However, this correlation is much weaker in the trade-wind regions and

in the stratocumulus-dominated region off the south American coast north of 20°S. This is largely explained by low variability in both cloud amount and LTS in the regions of weak $LTS - CF$ correlation is reduced (Fig. 10). Thus, even if LTS and CF are related in this region, it is easier for additional physical factors (or observational noise) to drown out signals in the regressions. Regions where the $LTS - CF$ correlation is strongest (Fig. 8(c,d)) are those where the variability in LTS and CF is strongest (Fig. 10).

It is interesting that the coastal SE Pacific region exhibits variability in CF and LTS that is markedly smaller than anywhere to the south and west, and anywhere in the NE Pacific stratocumulus region (Fig. 10). This is likely related to the influence of the Andes Cordillera which moderates variability in tropospheric temperatures over the far Eastern Pacific by blocking the propagation of the midlatitude baroclinic systems that are responsible for much of the daily-weekly variability in mid-tropospheric temperatures in the subtropics.

Temperature advection (Fig. 9) is only weakly correlated with $\overline{LWP}$, but is quite well correlated with CF, particularly in the stratocumulus to cumulus transition region of the NE Pacific (as found in Klein 1997), in the stratocumulus regions south of 20°S, and to the north of the equatorial cold tongue, where particularly strong cold advection results in strong surface forcing (deSzoeke and Bretherton 2004), and tropical instability waves provide important modulation of the surface fluxes (Thum et al. 2002). Finally, no significant correlations of free-tropospheric moisture with CF were found anywhere in the NE or SE Pacific, except to the north of the equatorial cold tongue.

Fig. 11 demonstrates that z_i has very little correlation with $\overline{LWP}$, and only weak correlation with CF. The latter is surprising given the excellent correlation for the means (Fig. 8(b)). In addition, LTS and z_i are strongly negatively correlated (r=-0.4 to -0.7) in the regions where LTS and CF are strongly positively correlated (Fig. 12), which makes the lack of $z_i - CF$ correla-

tion in these areas puzzling. Although MBL depth is clearly influenced by LTS on daily-weekly timescales, it does not appear to be the z_i fluctuations themselves that are modulating CF. We examine possible inferences that can be made from this in Section 4d.

Figure 13 shows that cloud fraction and homogeneity are generally positively correlated throughout the regions of extensive low cloud cover. This is consistent with the Gaussian-s model (see Part I of this study) whereby cloud fraction and homogeneity are uniquely linked. The cloud homogeneity γ_{LWP} is found to negatively correlate with z_i, especially over the NE Pacific, suggesting that while z_i may not be the primary modulator of CF on the daily-weekly timescale, it influences mesoscale spatial variability in some regions. This may be because thermodynamic and cloud inhomogeneity is closely tied to the characteristic lengthscale of mesoscale cells, which is well correlated with z_i, particularly in the regions of extensive stratocumulus clouds (not shown). We return to this scaling of mesoscale features with MBL depth in Section 5.

c. Dominant timescales of variability

To assess the controlling mechanism for the modulation of clouds and large scale forcings on daily to monthly timescales, we use autocorrelation analysis on the daily timeseries for each $5\times5^{\circ}$ gridbox. Standard harmonic analysis is precluded because each gridbox does not contain data on every day during the analysis period. Autocorrelation data are obtained for each series at lags of 1-30 days, and for each series with at least 50% of the maximum possible data points we estimate the non-zero lag at which the series becomes best correlated again with itself. This lag is the dominant timescale and coincides with the period of the dominant mode of variability (it would be equal to the wavelength for a sinusoidal signal). This timescale is plotted in Fig. 14 as a function of

latitude. Several key points are noted. First, the dominant timescales are mostly in the range 7-12 days and do not vary strongly with latitude. Spectral analysis of midlatitude geopotential fields (Fraedrich and Bottger 1978) reavels a dominant mode of variability with an approximate 10 day period corresponding to eastward propagating long waves. Hakim (2003) demonstrates that these waves are, in fact, midlatitude wave packets forming in the North Pacific storm track, and that they frequently penetrate deep into the subtropics, and sometimes the tropics. Second, the timescales of cloud and forcing parameters are approximately equal suggesting that the variability of cloud on daily-weekly timescales is largely modulated by large-scale meteorology. Hovmoller plots of the NCEP and cloud variables (not shown) do show eastward propagating signals consistent with Fraedrich and Bottger (1978) and Hakim (2003), especially outside of the deep tropics. In the deep tropics (10°S-10°N), a combination of stationary and westward propagating features dominate the variability in both cloud and large-scale meteorology.

d. What controls cloud fraction and homogeneity variations?

Two hypotheses for why increasing LTS tends to increase the cloud fraction and LWP heterogeneity both center around the concept that short timescale LTS fluctuations affect the MBL inversion strength in addition to the MBL depth. For a fixed amount of turbulent kinetic energy, an increase in inversion strength lead to a reduction in entrainment. The two hypotheses are that:

(i) reduced entrainment associated with increased LTS leads to a reduction in MBL depth. Shallower MBLs are more likely to remain well-mixed (Bretherton and Wyant 1997; Wood and Bretherton 2004) so that the cloud layer remains connected to the oceanic moisture supply. Deeper MBLs on the other hand are more likely to decouple, and this decoupling results in cloud breakup

and increasing heterogeneity;

(ii) reduced entrainment associated with increased LTS lessens the incorporation of warm, dry air into the MBL. A cooler, moister boundary layer is more favorable for the maintenance of cloud.

On the seasonal mean timescale it appears that hypothesis (i) is supported by the data, with the largest mean CFs being associated with the greatest LTS and shallowest MBLs. This suggests that the mean LTS is an indicator of seasonal mean MBL depth which, in turn, determines the climatological cloud amount and homogeneity. However, the regression analysis of daily data does not support (i) on short timescales because of the general lack of correlation between z_i and CF on these timescales. However, LTS variations on short timescales are clearly affecting CF, which suggests the tentative conclusion that although increased LTS is associated with shallow z_i, it is LTS itself, rather than the MBL depth *per se* that controls the cloud fraction variability on short timescales. This leaves the possibility that hypothesis (ii) is the key explanation for increased LTS increasing cloud fraction fraction and homogeneity on short timescales. However, there is no available data at present to examine this relationship on short timescales because we do not have entrainment estimates at this high temporal resolution. We hope that an extensive Lagrangian-type analysis of high temporal resolution geostationary satellite data (e.g. Pincus et al. 1997) may be able to address this hypothesis on short timescales, because MBL growth can be examined along airmass trajectories.

5. Scaling of mesoscale variability

Figure 15 shows the median characteristic cell lengthscale λ_1 binned as a function of MBL depth z_i. When the MBL depth is greater than $\sim$ 600 m, the cells tend to organize with preferred aspect ratios (horizontal:vertical cell scale) in the range 30-40. There is considerable variation of this

aspect ratio from scene to scene, as might be expected if some considerable time is required for cells to equilibrate at their preferred scale (see e.g. Shao and Randall 1996). For example, for MBLs between 1200-1300 m deep, the 25th, 50th and 75th percentiles of λ_1 are 31, 41 and 63 km respectively, indicating a considerable range within each z_i class. However, it is possible that this spread is caused by random errors and ambiguity in the determination of λ_1 from the MODIS scenes. It could also be caused by the MCC growth timescale being comparable or longer than the MBL growth timescale. Lagrangian studies of evolving MCC using geostationary satellites may prove to be a useful tool to resolve these issues. The relation $\lambda_1 = 4.6(z_i - 550)^{1/3}$ (z_i in m and λ_1 in km) fits the data quite well and is shown in Fig. 15.

For z_i lower than $\sim$ 800 m there is a marked decrease in λ_1 suggesting that the growth of MCC is not favored in well-mixed shallow MBLs. Indeed, for $z_i < 600$ m MCC is seldom observed in our dataset. This provides some support for the conceptual model proposed by Shao and Randall (1996) whereby the production of MCC requires the presence of a stable layer in the middle of the cloud-topped MBL. Such stable layers are associated with the decoupling of the MBL, a phenomenon rarely observed when $z_i < 600$ m or so. It is hypothesized that the presence or absence of MCC might be a sensitive indicator of MBL decoupling. To be tested, this speculation would require additional investigation with a combination of satellite and in-situ data. Synthetic aperture radar can readily detect patterns of variability in surface wind that correspond to MCC in cold air outbreaks. The presence or absence of such patterns in subtropical MCC may be a sensitive indicator of MBL decoupling, and is worthy of further investigation.

An automatic classification procedure described in Part I allows us to determine the scenes containing MCC, and for these scenes, whether the MCC is of open or closed type. With this classification we find that the $\lambda_1 - z_i$ relationships for open and for closed cells are very similar

when $z_i > 800$ m (not shown). However, closed cells are much the more common type of MCC when the MBL is shallower (constituting 83% of the MCC scenes when $800 < z_i < 1200$, but only 38% in MBLs deeper than 2000 m). From this we hypothesize that the cell scale is not determined by whether the MCC is open or closed, but that open MCC becomes more favorable in deeper MBLs. Although the Shao and Randall conceptual model for closed MCC may indeed be driven by cloud top radiative cooling, it is difficult to account for open MCC with this mechanism. This leads one to wonder if it is purely coincidental that there appears to be no systematic difference between the median aspect ratios in open and closed MCC. Or, is a single mechanism responsible for the generation of the two types of MCC? Large eddy simulations (de Roode et al. 2004) with extensive domains suggest that radiative cooling is not necessary for the generation of MCC (see also the introduction of Part I of this study). Instead, particular configurations of the buoyancy flux profile lead to mesoscale fluctuations. Such profiles may be caused by latent heating and drizzle, in addition to radiative cooling. Another possibility is that because open MCC is often formed by transition from closed MCC, its dominant scale could be determined during the closed phase and simply retained after the transition to open MCC.

The MCC characteristic lengthscale λ_1 is an important parameter because it is closely tied to the degree of mesoscale variance in saturation excess. In Part I a method was presented to estimate the standard deviation of the saturation excess σ_s in the cloud layer, using MODIS observations of the LWP pdf. In Figure 16 we show plots of median σ_{LWP} and median estimated σ_s against cell scale λ_1 and MBL depth z_i. Both σ_{LWP} and σ_s increase as λ_1 increases, indicating that enhanced mesoscale variance in saturation excess (relative humidity) and consequently LWP is associated with larger cells. Near-linear relationships are found between $\sigma_{LWP} - z_i$ and $\sigma_s - z_i$. Also shown are median values from a number of intensive field programs (Wood and Taylor 2001; Wood

et al. 2002; Bretherton et al. 2004) in subtropical MBLs in the NE Atlantic (ASTEX), NE Pacific (FIRE) and SE Pacific (EPIC). Aircraft observations and microwave radiometer LWP are derived from reliable measurements and provide support that a general scaling exists between mesoscale variability and MBL depth, and is intimately coupled through the mechanism of MCC cell growth.

Finally, we use the MODIS data to examine the parameterization of critical relative humidity as used in the Met. Office GCM. Critical relative humidity is defined as the relative humidity at which clouds start to form in a numerical model gridbox, and is an important parameter used to determine the fractional coverage of stratiform clouds. It is related to σ_s via

$$RH_C = 1 - \frac{\sigma_s \sqrt{6}}{a q_{sat}(\overline{T_l}, p)} \tag{2}$$

where a is a fairly weak function of temperature, $\overline{T_l}$ is the liquid temperature, p is the pressure, and q_{sat} is the saturation specific humidity (see Part I of this study). Figure 17 demonstrates that the median RH_C falls off linearly with height, consistent with the imposed height trend used in the runs with fixed RH_C in the climate configuration of the Met Office GCM (Cusack et al. 1999). This behavior is consistent with a broadening of the saturation excess pdf in deeper MBLs. However, observationally derived values tend to be markedly lower than the GCM parameterization, but a recent scheme to prognose RH_C using scaling arguments (Cusack et al. 1999, see also Part I of this study) has been found to reduce RH_C in the subtropics to values much closer to the observations. Recent numerical experiments to evaluate cloud feedback under a doubling of CO_2 (Williams et al. 2003) demonstrate that different parameterizations of RH_C have a large impact upon the net response of clouds to climate change. The MODIS observations provide a useful constraint for such parameterizations.

6. Discussion and conclusions

In Part II of this study we have presented an initial attempt at the production of a climatology of low cloud mesoscale variability over the NE and SE Pacific Ocean, using 1 km resolution data from MODIS. We have used a number of parameters, discussed in more depth in Part I of the study, that best characterize the mesoscale spatial variability in MBL cloud. We find that three parameters (CF, mean in-cloud liquid water path, and the square of the ratio of the mean to standard deviation of the cloud-only liquid water path) provide a reasonably complete description of the one point statistics of cloud liquid water path mesoscale spatial variability. We also find that cloud homogeneity is strongly coupled with CF, and that the spatial variability in cloud can be coupled quite effectively to variability in the underlying thermodynamic parameters using a simple Gaussian model of saturation excess.

We have examined how these parameters vary in relation to large-scale forcings from NCEP reanalysis products, using both regressions of daily gridded data and by examining the geographical variability of mean values. The results suggests that both cloud cover and the mesoscale spatial variability within cloud are modulated by fluctuations in large-scale meteorological variables, particularly LTS (Klein and Hartmann 1993) and temperature advection (Klein 1997). In many places, most notably off the coast of Peru, cloud cover and spatial variability are not strongly correlated with any of the meteorological variables examined, but this is due to the very low degree of daily-weekly variability in the lower tropospheric meteorology to the west of the Andes chain. The mean cloud fraction in the regions of low daily-weekly variability do well correlated with the lower tropospheric stability.

While there are very good relationships between $2.5\times2.5^{\circ}$ means of CF and both LTS and

MBL depth, the regression analysis shows that CF variations are not strongly correlated with z_i on short timescales. This suggests that it may be variation in entrainment rate, rather than z_i *per se* that controls the cloud fraction.

Cloud homogeneity γ_{LWP} correlates with z_i in regions where the $CF - z_i$ correlations are poor, suggesting that the mesoscale variability may indeed be more strongly controlled by MBL depth than entrainment rate. The observed couplings between mesoscale LWP/saturation excess variance, the characteristic lengthscale of the mesoscale cellular convection (MCC), and the MBL depth, are good evidence that there may exist well-defined scalings between the MBL depth and the thermodynamic/cloud spatial variability properties in the MBL. These may be useful, both in offering insight into the processes controlling mesoscale spatial variability in MBL clouds, and for future development of parameterizations to account for such variability.

Finally, we can demonstrate schematically how the transition from shallow stratus-topped MBLs through stratocumulus to the deeper trade-wind MBLs occurs in the context of the Gaussian model linking saturation excess and cloud properties (Fig. 18). As we discussed in Part I of this study, we can represent the observed cloud mesoscale properties ($\overline{LWP}$, CF, γ_{LWP}) by assuming a Gaussian distribution of saturation excess and a locally adiabatic model. Equivalently, this can be conceptualized using a Gaussian pdf of the LCL and an adiabatic profile for $z < z_i$, with no cloud in the fractional area where $LCL > z_i$. The evolution of the clouds and their mesoscale structure along equatorward trajectories can be conceptualized as a rising of z_i, a more rapid rising of the mean LCL, and an increase in the width of the pdf of the LCL (or saturation excess). In part I, we saw that the the mean LWP is roughly conserved in the transition from stratus to trade cumulus, and we suggested that this may be related to active feedbacks, possibly involving drizzle and longwave radiation. The geographical variability of $\overline{LWP}$ (Fig. 1) confirms this relatively

narrow range of $\overline{LWP}$. The evolution of the LCL pdf (or equivalently the saturation deficit pdf) provides a theoretical framework for the observed changes in the mesoscale variability of clouds in the subtropics. Recent advances in the parameterization of cloud-topped MBLs (e.g. Martin et al. 2000) diagnose MBL depth, and this could be used to parameterize the saturation excess pdf width, thereby accounting for unresolved subgrid variability in cloud structure (Fig. 16) in a physically consistent manner.

References

Betts, A. K.: 1989, Mean inversion strength of the convective boundary layer over the oceans. *Quart. J. Roy. Meteorol. Soc.*, **115**, 997–998.

Betts, A. K. and W. Ridgway: 1988, Coupling of the radiative, convective, and surface fluxes over the equatorial pacific. *J. Atmos. Sci.*, **45**, 522–536.

Bretherton, C. S., S. K. Krueger, M. C. Wyant, P. Bechtold, E. vanMeijgaard, B. Stevens, and J. Teixeira: 1999, A gcss boundary layer model intercomparison study of the first astex lagrangian experiment. *Bound. Layer Meteorol.*, **93**, 341–380.

Bretherton, C. S. and R. Pincus: 1995, Cloudiness and marine boundary layer dynamics in the ASTEX lagrangian experiments. Part I: Synoptic setting and vertical structure. *J. Atmos. Sci.*, **52**, 2707–2723.

Bretherton, C. S., T. Uttal, C. W. Fairall, S. E. Yuter, R. A. Weller, D. Baumgardner, K. Comstock, and R. Wood: 2004, The EPIC 2001 stratocumulus study. *Bull. Am. Meteorol. Soc.*, **85**, 967–977.

Bretherton, C. S. and M. C. Wyant: 1997, Moisture transport, lower-tropospheric stability, and decoupling of cloud-topped boundary layers. *J. Atmos. Sci.*, **54**, 148–167.

Cahalan, R. F., W. Ridgway, W. J. Wiscombe, T. L. Bell, and J. B. Snider: 1994, The albedo of fractal stratocumulus clouds. *J. Atmos. Sci.*, **51**, 2434–2455.

Cusack, S., J. M. Edwards, and R. Kershaw: 1999, Estimating the subgrid variance of saturation, and its parametrization for use in a gcm cloud scheme. *Quart. J. Roy. Meteorol. Soc.*, **12**, 3057–3076.

Dai, A. and C. Deser: 1999, Diurnal and semidiurnal variations in global surface wind and divergence fields. *J. Geophys. Res.*, **104**, 31109–31125.

de Roode, S. R. and P. G. Duynkerke: 1997, Observed lagrangian transition of stratocumulus into cumulus during ASTEX: mean state and turbulence structure. *J. Atmos. Sci.*, **54**, 2157–2173.

de Roode, S. R., P. G. Duynkerke, and H. J. Jonker: 2004, Large eddy simulation: how large is large enough? *J. Atmos. Sci.*, **61**, 403–421.

deSzoeke, S. P. and C. S. Bretherton: 2004, Quasi-lagrangian large eddy simulations of cross-equatorial flow in the east pacific atmospheric boundary layer. *J. Atmos. Sci.*, submitted.

Fraedrich, K. and H. Bottger: 1978, A wavenumber-frequency analysis of the 500 mb geopotential at $50^\circ n$. *J. Atmos. Sci.*, **35**, 745–750.

Garreaud, R. D. and R. Muñoz: 2004, The diurnal cycle in circulation and cloudiness over the subtropical southeast pacific: A modeling study. *J. Clim.*, in press.

Hakim, G. J.: 2003, Developing wave packets in the north pacific storm track. *Mon. Wea. Rev.*, **131**, 342–355.

Kistler, R., E. Kalnay, W. Collins, S. Sana, G. White, J. Woolen, M. Chelliah, W. Ebisuzaki, M. Kanamitsu, V. Kousky, H. van den Dool, R. Jenne, and M. Fiorino: 2001, The ncep/ncar 50-year reanalysis. *Bull. Am. Meteorol. Soc.*, **82**, 247–267.

Klein, S. A.: 1997, Synoptic variability of low-cloud properties and meteorological parameters in the subtropical trade wind boundary layer. *J. Climate*, **10**, 2018–2039.

Klein, S. A. and D. L. Hartmann: 1993, The seasonal cycle of low stratiform clouds. *J. Climate*, **6**, 1588–1606.

Kuo, H.-C. and W. H. Schubert: 1988, Stability of cloud-topped boundary layers. *Quart. J. Roy. Meteorol. Soc.*, **114**, 887–916.

Larson, V. E., R. Wood, P. R. Field, J.-C. Golaz, T. H. Vonder Haar, and W. R. Cotton: 2001, Systematic biases in the microphysics and thermodynamics of numerical models that ignore subgrid-scale variability. *J. Atmos. Sci.*, **58**, 1117–1128.

Martin, G. M., M. R. Bush, A. R. Brown, A. P. Lock, and R. N. B. Smith: 2000, A new boundary layer mixing scheme. Part II: Tests in climate and mesoscale models. *Mon. Wea. Rev.*, **128**, 3200–3217.

Park, S., C. B. Leovy, and M. A. Rozendaal: 2004, A new single column marine boundary layer cloud model. *J. Atmos. Sci.*, submitted.

Pincus, R., M. B. Baker, and C. S. Bretherton: 1997, What controls stratocumulus radiative properties? lagrangian observations of cloud evolution. *J. Atmos. Sci.*, **54**, 2215–2236.

Pincus, R. and S. A. Klein: 2000, Unresolved spatial variability and microphysical process rates in large scale models. *J. Geophys. Res.*, **105**, 27059–27066.

Reynolds, R. W. and T. M. Smith: 1994, Improved global sea surface temperature analyses using optimum interpolation. *J. Clim.*, **7**, 929–948.

Rossow, W. B., C. Delo, and B. Cairns: 2002, Implications of the observed mesoscale variations of clouds for earth's radiation budget. *J. Clim.*, **15**, 557–585.

Rotstayn, L. D.: 2000, On the ”tuning” of autoconversion parameterizations in climate models. *J. Geophys. Res.*, **105**, 15,495–15,507.

Rozendaal, M. A., C. B. Leovy, and S. A. Klein: 1995, An observational study of the diurnal cycle of marine stratiform cloud. *J. Clim.*, **8**, 1795–1809.

Schubert, W. H., J. S. Wakefield, E. J. Steiner, and S. K. Cox: 36, Marine stratocumulus convection. part i: Governing equations and horizontally homogeneous solutions. *J. Atmos. Sci.*, 1286–1307.

Shao, Q. and D. A. Randall: 1996, Closed mesoscale cellular convection driven by cloud-top radiative cooling. *J. Atmos. Sci.*, **53**, 2144–2165.

Slingo, J. M.: 1980, A cloud parameterization scheme derived from GATE data for use with a numerical model. *Quart. J. Roy. Meteorol. Soc.*, **106**, 774–770.

— 1987, The development and verification of a cloud prediction scheme for the ECMWF model. *Quart. J. Roy. Meteorol. Soc.*, **113**, 899–927.

Thum, N., S. K. Esbensen, D. B. Chelton, and M. J. McPhaden: 2002, Air-sea heat exchange along the northern sea surface temperature front in the eastern tropical Pacific. *J. Clim.*, **23**, 3361–3378.

Williams, K. D., M. A. Ringer, and C. A. Senior: 2003, Evaluating the cloud response to climate change and current climate variability. *Clim. Dyn.*, **20**, 705–721.

Wood, R. and C. S. Bretherton: 2004, Boundary layer depth, entrainment and decoupling in the cloud-capped subtropical and tropical marine boundary layer. *J. Clim.*, **17**, 3576–3588.

Wood, R., P. R. Field, and W. R. Cotton: 2002, Autoconversion rate bias in boundary layer cloud parameterizations. *Atmos. Res.*, **65**, 109–128.

Wood, R. and J. P. Taylor: 2001, Liquid water path variability in unbroken marine stratocumulus. *Quart. J. Roy. Meteorol. Soc.*, **127**, 2635–2662.

Figure Captions

Figure 1: Climatological mean value of $\overline{LWP}$ (a,b), CF (c,d), and climatological median value of γ_{LWP} (e,f) for all September/October MODIS scenes in the NE and SE Pacific.

Figure 2: Mean MBL depth (contours) and surface winds (arrows) for all warm cloud scenes in the NE (a) and SE (b) Pacific, Sept/Oct 2000.

Figure 3: Median values of the characteristic lengthscale for all scenes with $CF > 0.2$ for the NE (a) and SE (b) Pacific regions.

Figure 4: Fraction of MODIS scenes diagnosed as homogeneous cloud (a,b), closed MCC (c,d), and open MCC (e,f), for the NE and SE Pacific. The method used to determine the scene type is presented in Part I of this study.

Figure 5: Mean values of 850 hPa vertical wind w_{850} [cm s^{-1}] (a,b), LTS [K] (c,d), and temperature advection $\mathbf{U} \cdot \nabla SST$ [K day^{-1}] (e,f) for the corresponding MODIS scenes in the NE (left) and SE (right) Pacific during September/October 2000.

Figure 6: (a) Two-monthly mean values of MODIS scene cloud fraction as a function of LTS. Each point represents a single 2.5$\times$2.5° region. The dotted line shows the results of Klein and Hartmann (1993) and the dashed line the best fit to the MODIS data for the NE and SE Pacific. (b)

Cloud fraction as a function of MODIS-derived MBL depth.

Figure 7: Correlation coefficient between w_{850} and $\overline{LWP}$ (a,b), CF (c,d), and γ_{LWP} (e,f), for NE (left) and SE (right) Pacific MODIS data. In this, and all subsequent regression maps, shaded areas indicate regions where the correlations are significant at the 95% level. Non-significant correlations are not contoured.

Figure 8: Correlation coefficient between lower tropospheric stability LTS and $\overline{LWP}$ (a,b), CF (c,d), and γ_{LWP} (e,f), for NE (left) and SE (right) Pacific MODIS data.

Figure 9: Correlation coefficient between temperature advection and $\overline{LWP}$ (a,b), CF (c,d), and γ_{LWP} (e,f), for NE (left) and SE (right) Pacific MODIS data.

Figure 10: Standard deviation of daily mean cloud fraction σ_{CF} (a,b), 850 hPa vertical wind $\sigma_{\omega_{850}}$ [cm s^{-1}] (c,d), lower tropospheric stability σ_{LTS} [K] (e,f), and temperature advection σ_{TA} [K day^{-1}] in the NE and SE Pacific.

Figure 11: Correlation coefficient between MBL depth and $\overline{LWP}$ (a,b), CF (c,d), and γ_{LWP} (e,f), for NE (left) and SE (right) Pacific MODIS data.

Figure 12: Correlation coefficient between MBL depth and LTS for NE (a) and SE (b) Pacific data.

Figure 13: Correlation coefficient between cloud fraction CF and cloud homogeneity parameter γ_{LWP} for NE (a) and SE (b) Pacific data.

Figure 14: Dominant timescales for modulation of cloud structural parameters (a) and large scale forcings (b), plotted as a function of latitude for the NE and SE Pacific regions. Error bars show the 2-σ estimated uncertainty in the mean timescale, estimated using the available $5\times5^{\circ}$ grid-box data at each latitude.

Figure 15: Median characteristic cell lengthscale λ_1 binned by MBL depth z_i for all MODIS scenes (solid circles) over the NE and SE Pacific. The dotted lines denote aspect ratios of 20:1, 30:1 and 40:1. Error bars indicate the approximate sampling error in the median. The solid line indicates the fit described in the text.

Figure 16: Standard deviations of liquid water path σ_{LWP} (a,b) and saturation excess σ_s (c,d) plotted against cell scale λ_1 (a,c) and z_i (b,d). MODIS data are shown using solid (NE Pacific) and open (SE Pacific) circles, which represent median values for binned z_i ranges, with dashed and dotted lines respectively indicating 25th and 75th percentiles. Also shown are results from FIRE, EPIC and ASTEX (see text). The gray dashed lines in (b) and (d) are parameterizations described in the text.

Figure 17: Median critical relative humidity RH_C (with uncertainty) derived from MODIS observations, binned as a function of the mean height of the cloud layer. Also shown are the best fit line and the values used in fixed-RH_C configuration of the Met. Office GCM (Cusack et al. 1999).

Figure 18: Schematic figure showing the evolution of the MBL from the near coastal regions containing stratus to the NE of the subtropical high, through the stratocumulus regions where MCC initiates, to the trade wind regions dominated by clusters of cumulus clouds detraining stratiform cloud at the top of the MBL. The shaded region denotes the pdf of the LCL (cloud base height) which increases in both mean and variance downwind. The fraction of the pdf where $LCL < z_i$ contains cloud. This evolution of the LCL pdf (or equivalently the saturation deficit pdf) provides a theoretical framework for the observed changes in the mesoscale variability of clouds in the subtropics.

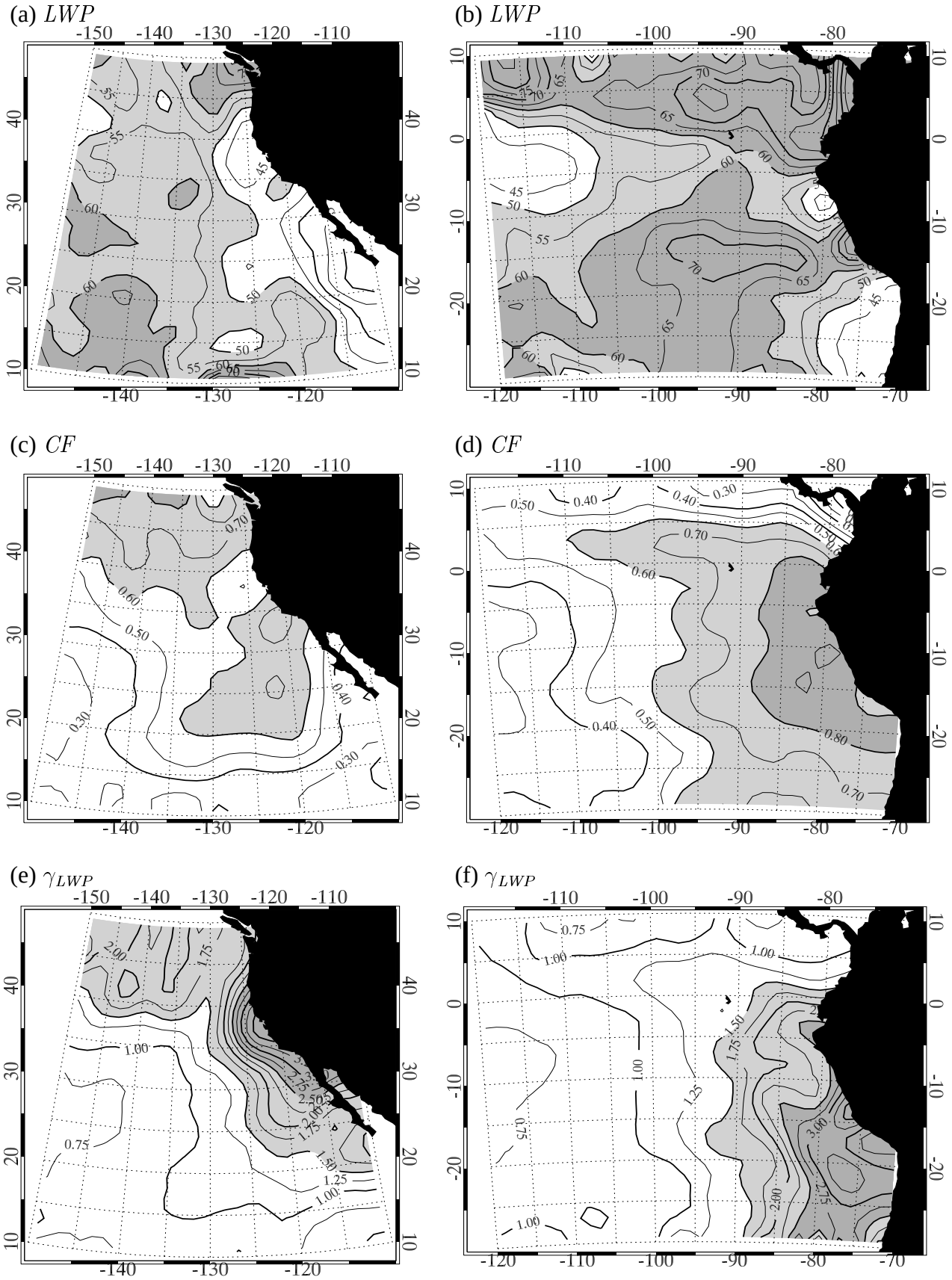

Figure 1:

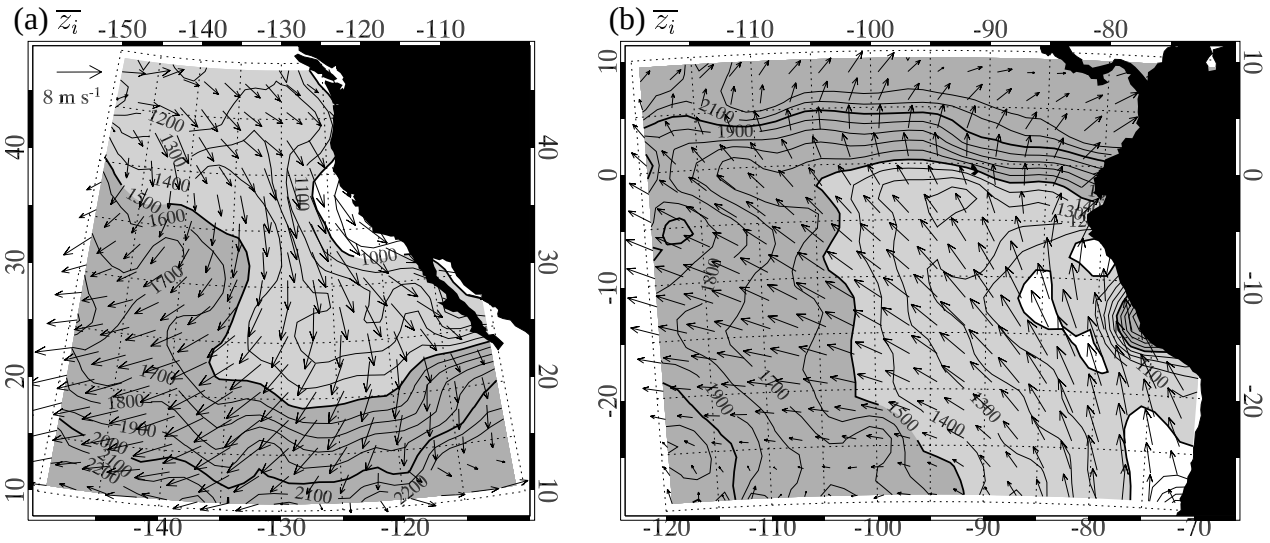
(a) $\overline{z_i}$
-150
-140
-130
-120
-110
8 m s-1
1200
1300
1400
1500
1600
1700
1800
1900
2000
2100
2200
1100
1000
40
30
20
10
(b) $\overline{z_i}$
-110
-100
-90
-80
10
0
-10
-20
2100
1900
1300
1500
1700
1400
-120
-70

Figure 2:

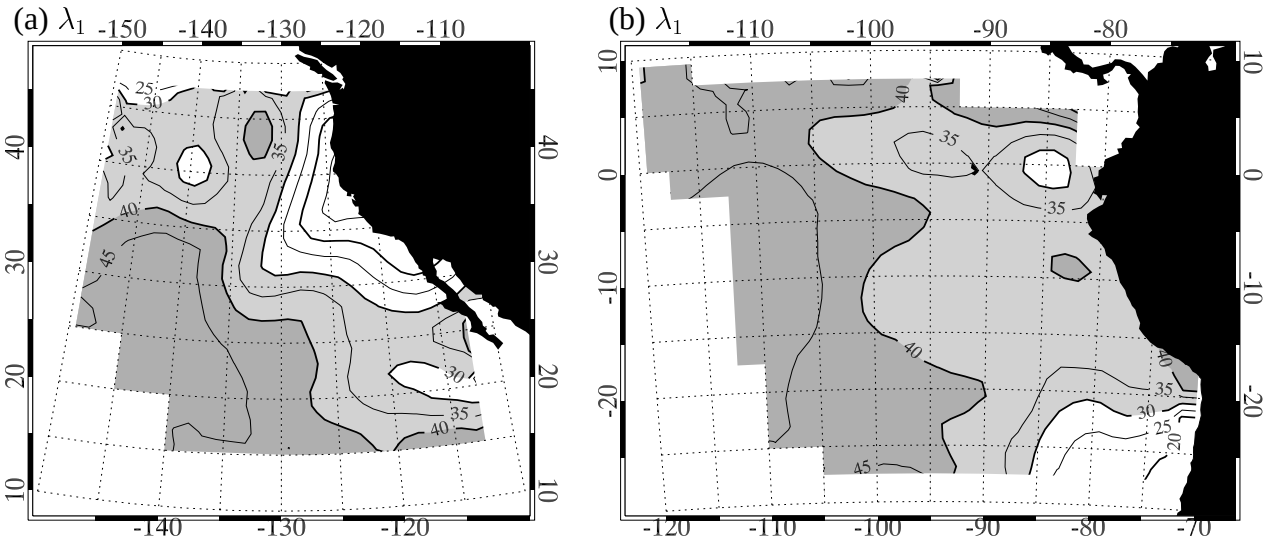
(a) λ_1
-150
-140
-130
-120
-110
40
30
20
10
25
30
35
40
45
(b) λ_1
-110
-100
-90
-80
10
0
-10
-20
-120
-70
35
40
45

Figure 3:

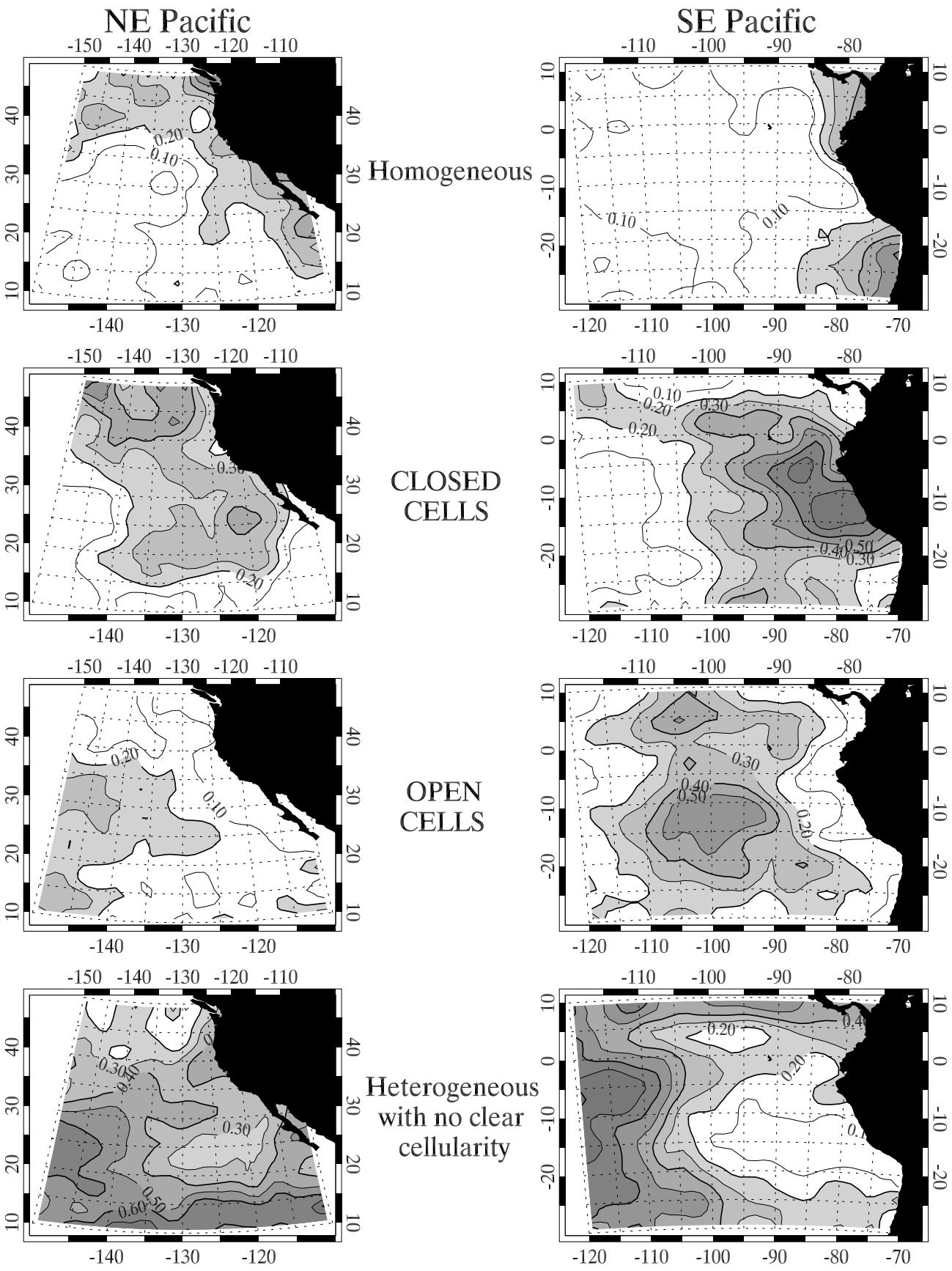
NE Pacific
SE Pacific
Homogeneous
CLOSED CELLS
OPEN CELLS
Heterogeneous with no clear cellularity

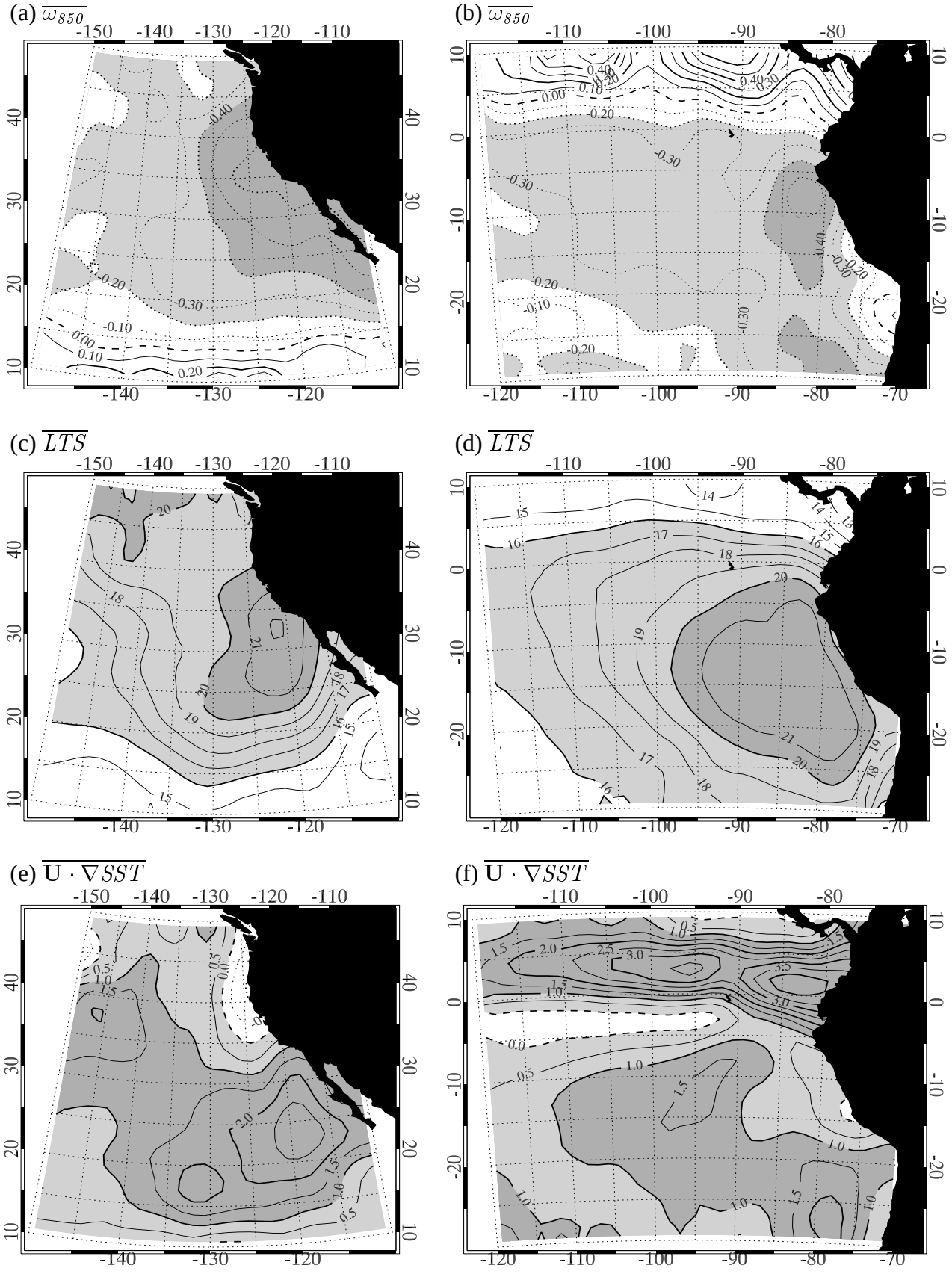
(a) $\overline{\omega_{850}}$
(b) $\overline{\omega_{850}}$
(c) $\overline{LTS}$
(d) $\overline{LTS}$
(e) $\overline{\mathbf{U} \cdot \nabla SST}$
(f) $\overline{\mathbf{U} \cdot \nabla SST}$

Figure 5:

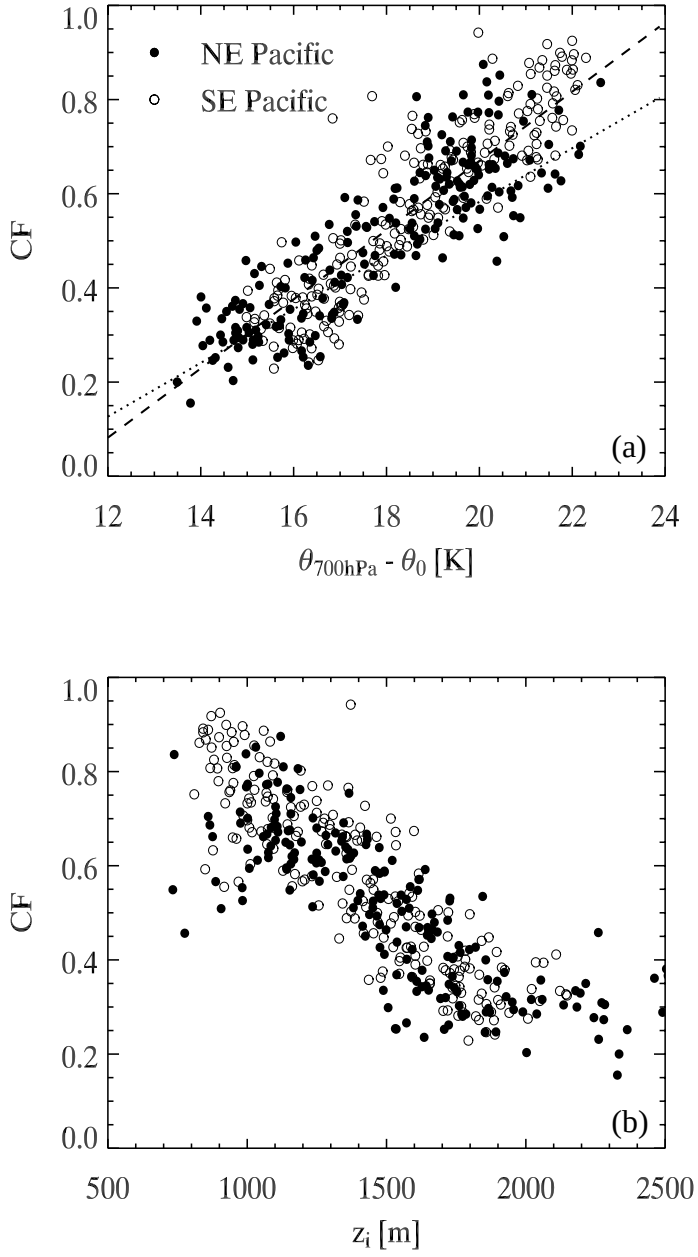

Figure 6:

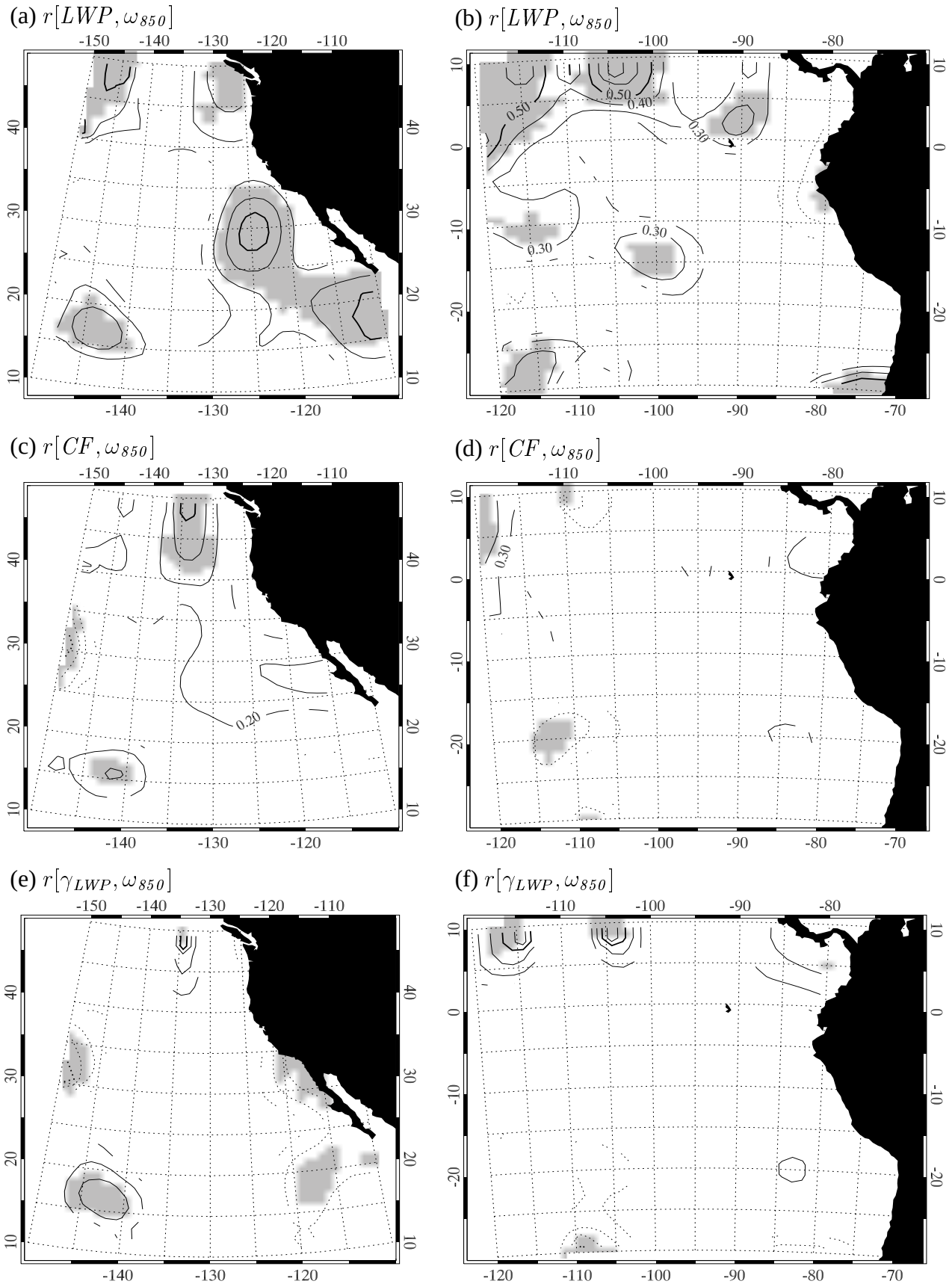
(a) $r[LWP, \omega_{850}]$
(b) $r[LWP, \omega_{850}]$
(c) $r[CF, \omega_{850}]$
(d) $r[CF, \omega_{850}]$
(e) $r[\gamma_{LWP}, \omega_{850}]$
(f) $r[\gamma_{LWP}, \omega_{850}]$
0.50
0.40
0.30
0.20

Figure 7:

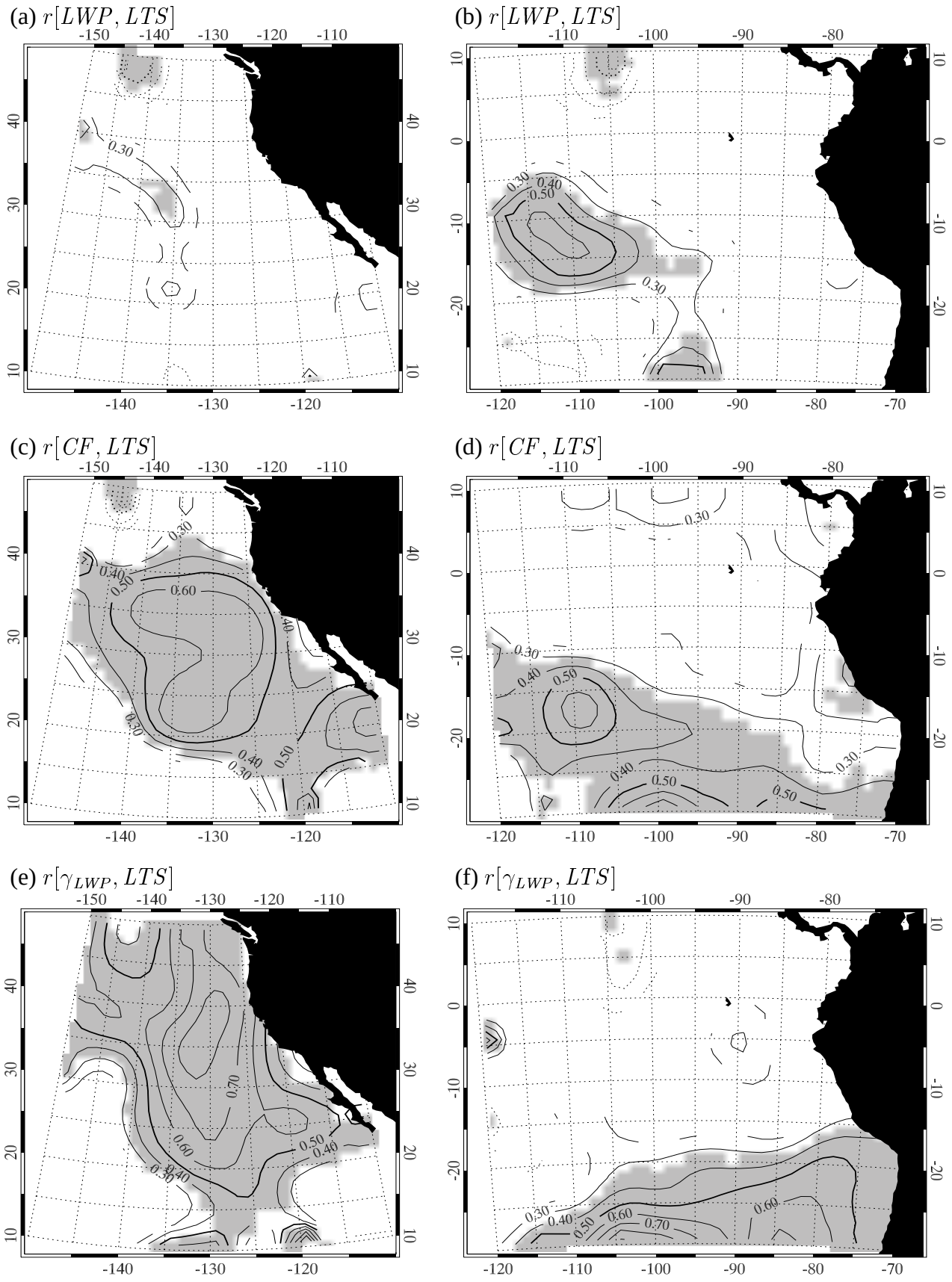
(a) $r[LWP, LTS]$
(b) $r[LWP, LTS]$
(c) $r[CF, LTS]$
(d) $r[CF, LTS]$
(e) $r[\gamma_{LWP}, LTS]$
(f) $r[\gamma_{LWP}, LTS]$

Figure 8:

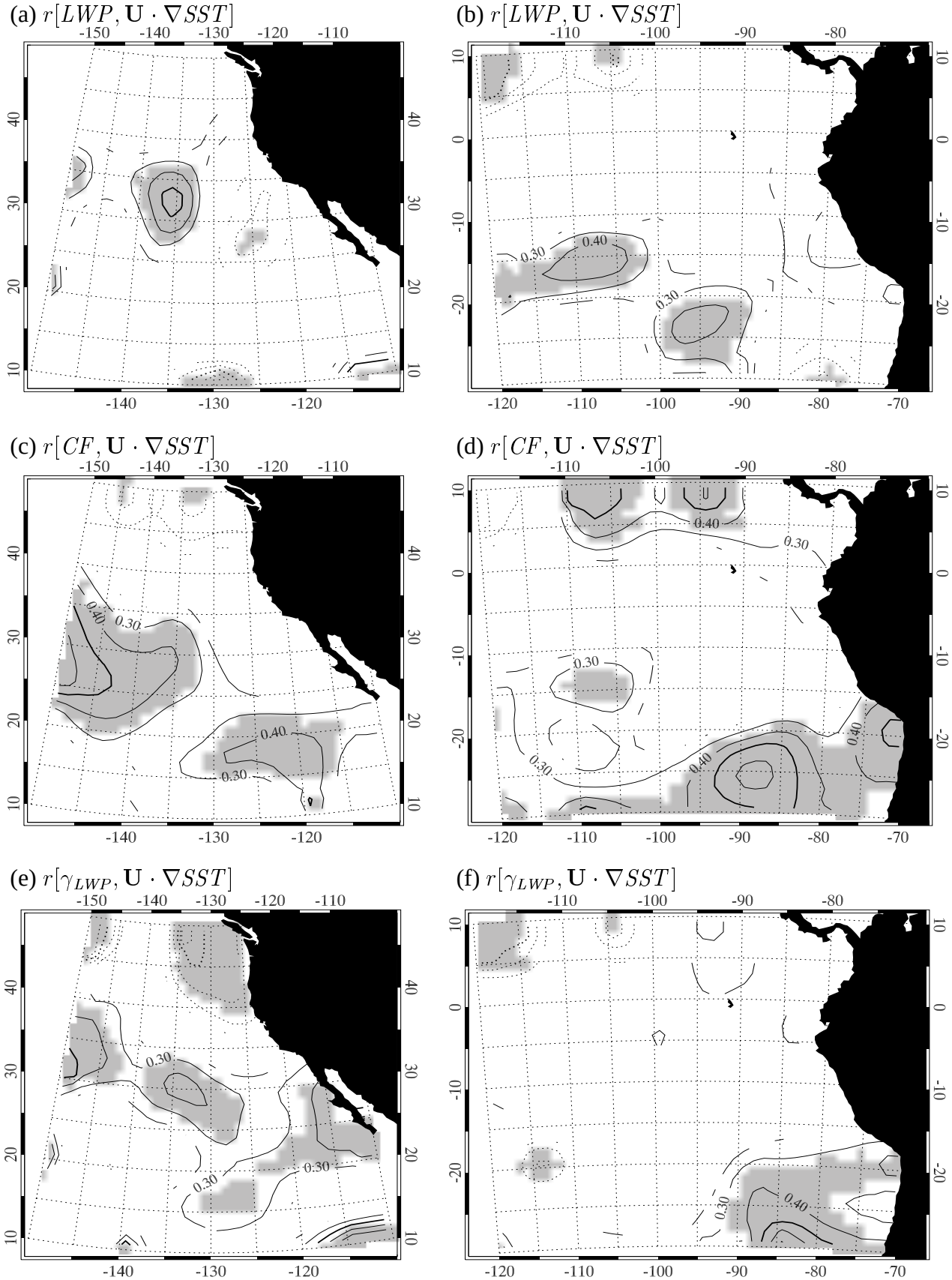
(a) $r[LWP, \mathbf{U} \cdot \nabla SST]$
(b) $r[LWP, \mathbf{U} \cdot \nabla SST]$
(c) $r[CF, \mathbf{U} \cdot \nabla SST]$
(d) $r[CF, \mathbf{U} \cdot \nabla SST]$
(e) $r[\gamma_{LWP}, \mathbf{U} \cdot \nabla SST]$
(f) $r[\gamma_{LWP}, \mathbf{U} \cdot \nabla SST]$
0.30
0.40

Figure 9:

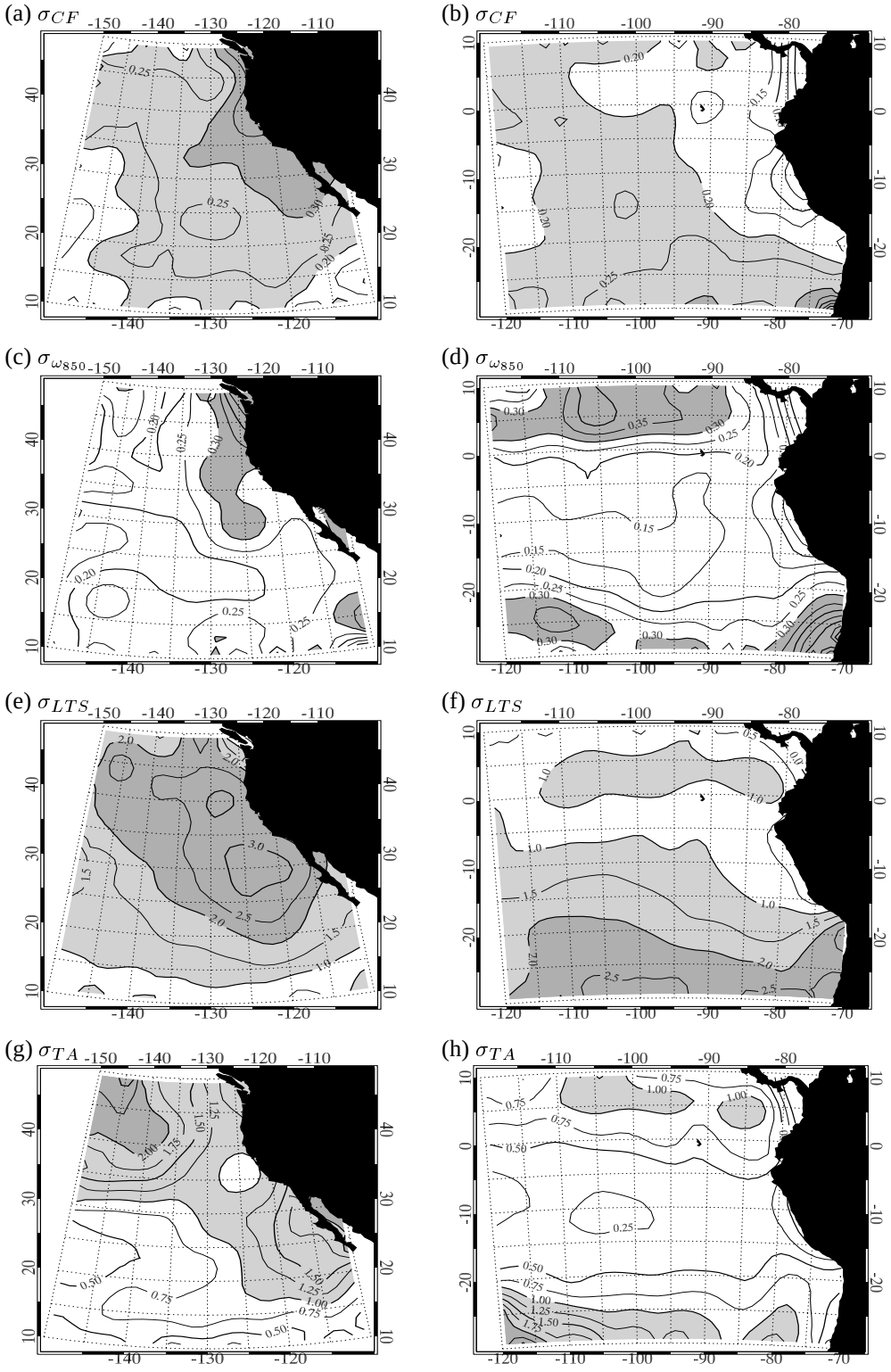
(a) σ_{CF}
(b) σ_{CF}
(c) $\sigma_{\omega 850}$
(d) $\sigma_{\omega 850}$
(e) σ_{LTS}
(f) σ_{LTS}
(g) σ_{TA}
(h) σ_{TA}

Figure 10:

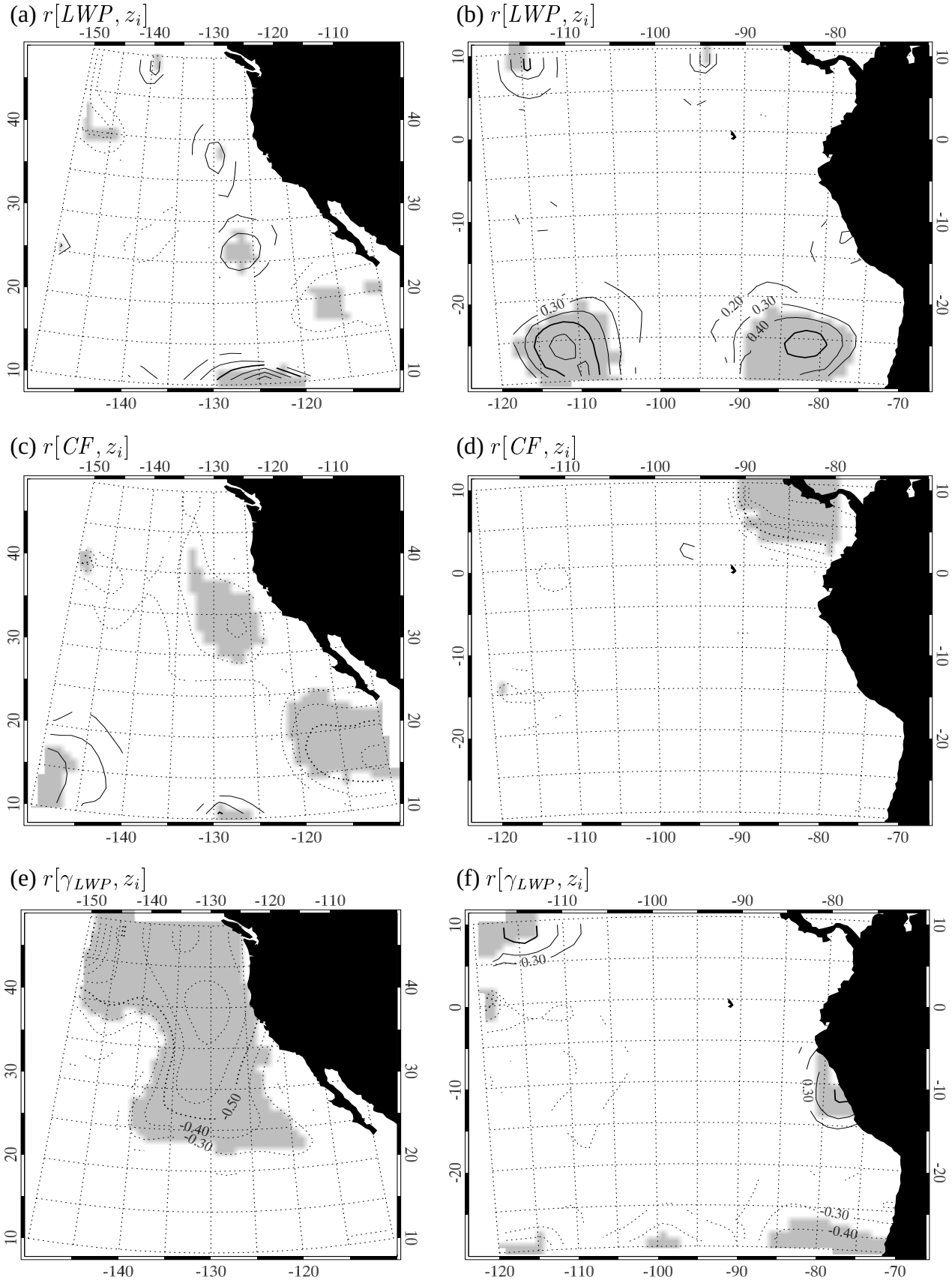
(a) $r[LWP, z_i]$
(b) $r[LWP, z_i]$
(c) $r[CF, z_i]$
(d) $r[CF, z_i]$
(e) $r[\gamma_{LWP}, z_i]$
(f) $r[\gamma_{LWP}, z_i]$
-150 -140 -130 -120 -110
-110 -100 -90 -80
-140 -130 -120
-120 -110 -100 -90 -80 -70
10 30 20 40
10 0 -10 -20
0.30
0.20
0.40
-0.50
-0.40
-0.30

Figure 11:

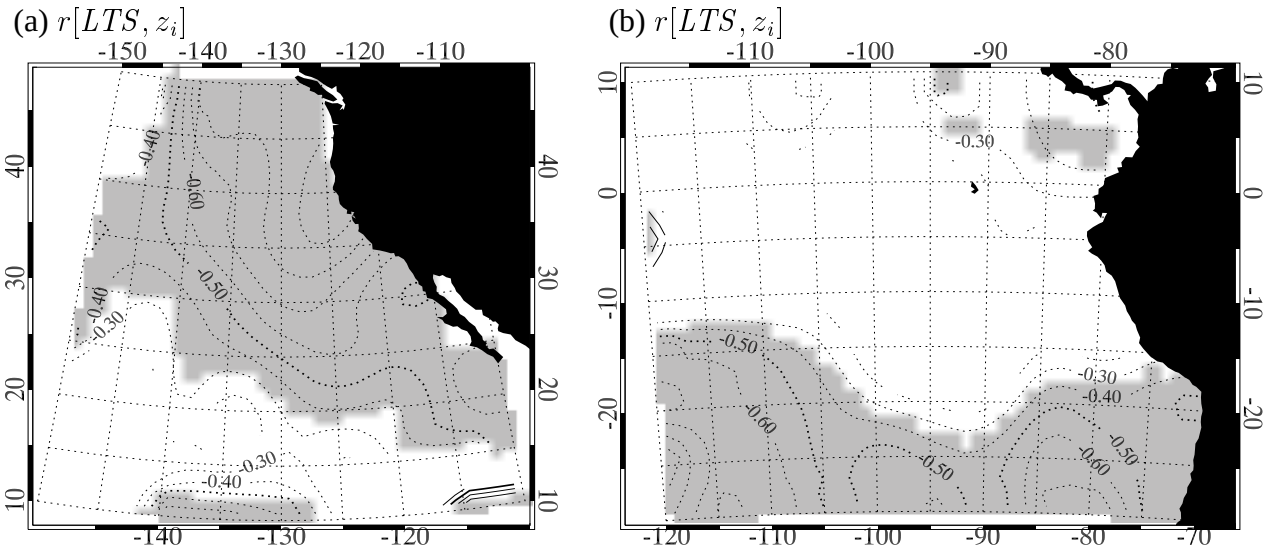
(a) $r[LTS, z_i]$
-150
-140
-130
-120
-110
40
30
20
10
-0.40
-0.60
-0.50
-0.40
-0.30
-0.30
-0.40
-140
-130
-120
(b) $r[LTS, z_i]$
-110
-100
-90
-80
10
0
-10
-20
-0.30
-0.50
-0.30
-0.40
-0.60
-0.50
-0.60
-0.50
-120
-110
-100
-90
-80
-70

Figure 12:

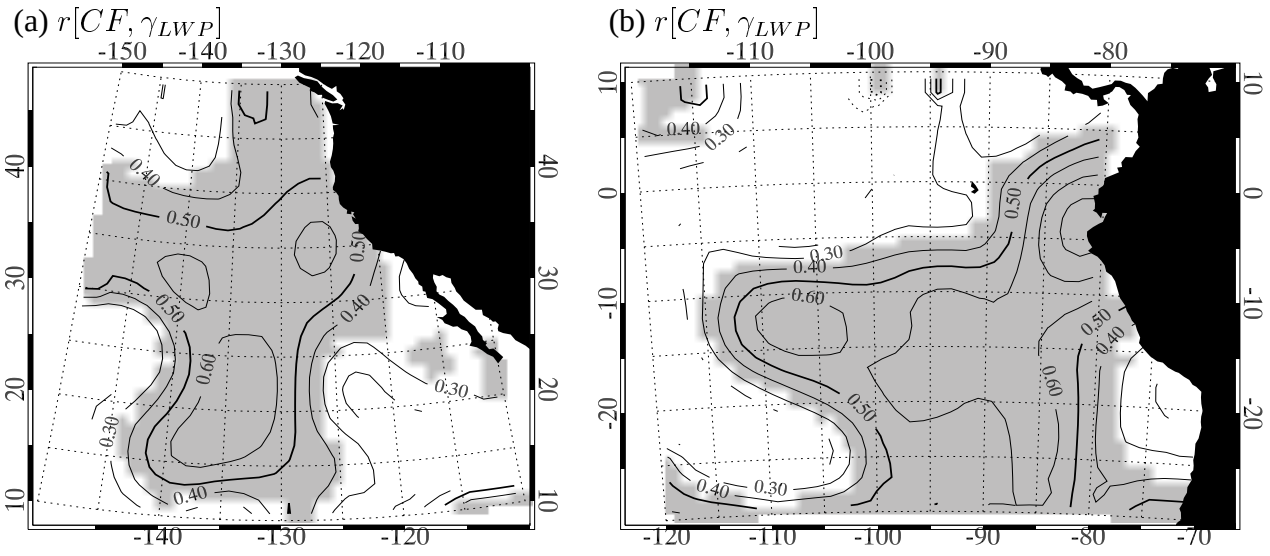
(a) $r[CF, \gamma_{LWP}]$
-150 -140 -130 -120 -110
40 30 20 10
-140 -130 -120
0.40 0.50 0.50 0.50 0.40 0.60 0.30 0.30 0.40
(b) $r[CF, \gamma_{LWP}]$
-110 -100 -90 -80
10 0 -10 -20
-120 -110 -100 -90 -80 -70
0.40 0.30 0.50 0.30 0.40 0.60 0.50 0.40 0.60 0.50 0.40 0.30

Figure 13:

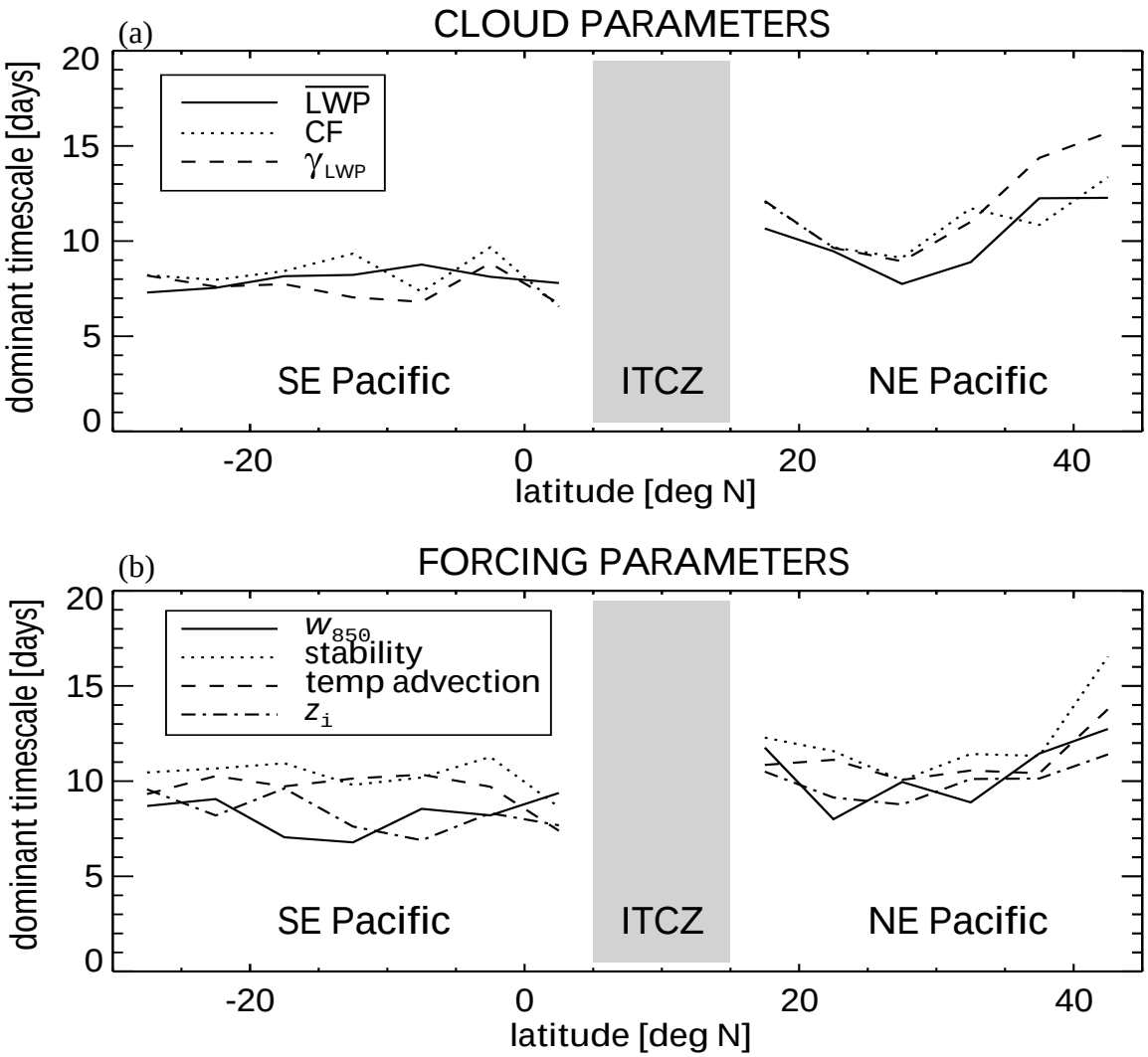
(a)
CLOUD PARAMETERS
dominant timescale [days]
LWP
CF
γ LWP
SE Pacific
ITCZ
NE Pacific
latitude [deg N]
(b)
FORCING PARAMETERS
w850
stability
temp advection
zi
SE Pacific
ITCZ
NE Pacific
latitude [deg N]

Figure 14:

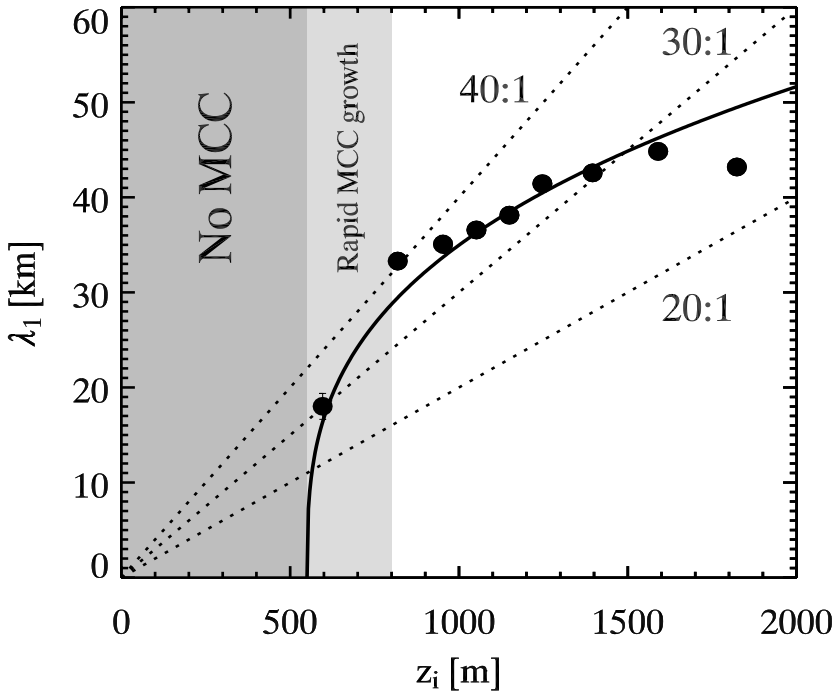
No MCC
Rapid MCC growth
30:1
40:1
20:1
λ_1 [km]
z_i [m]
0
10
20
30
40
50
60
0
500
1000
1500
2000

Figure 15:

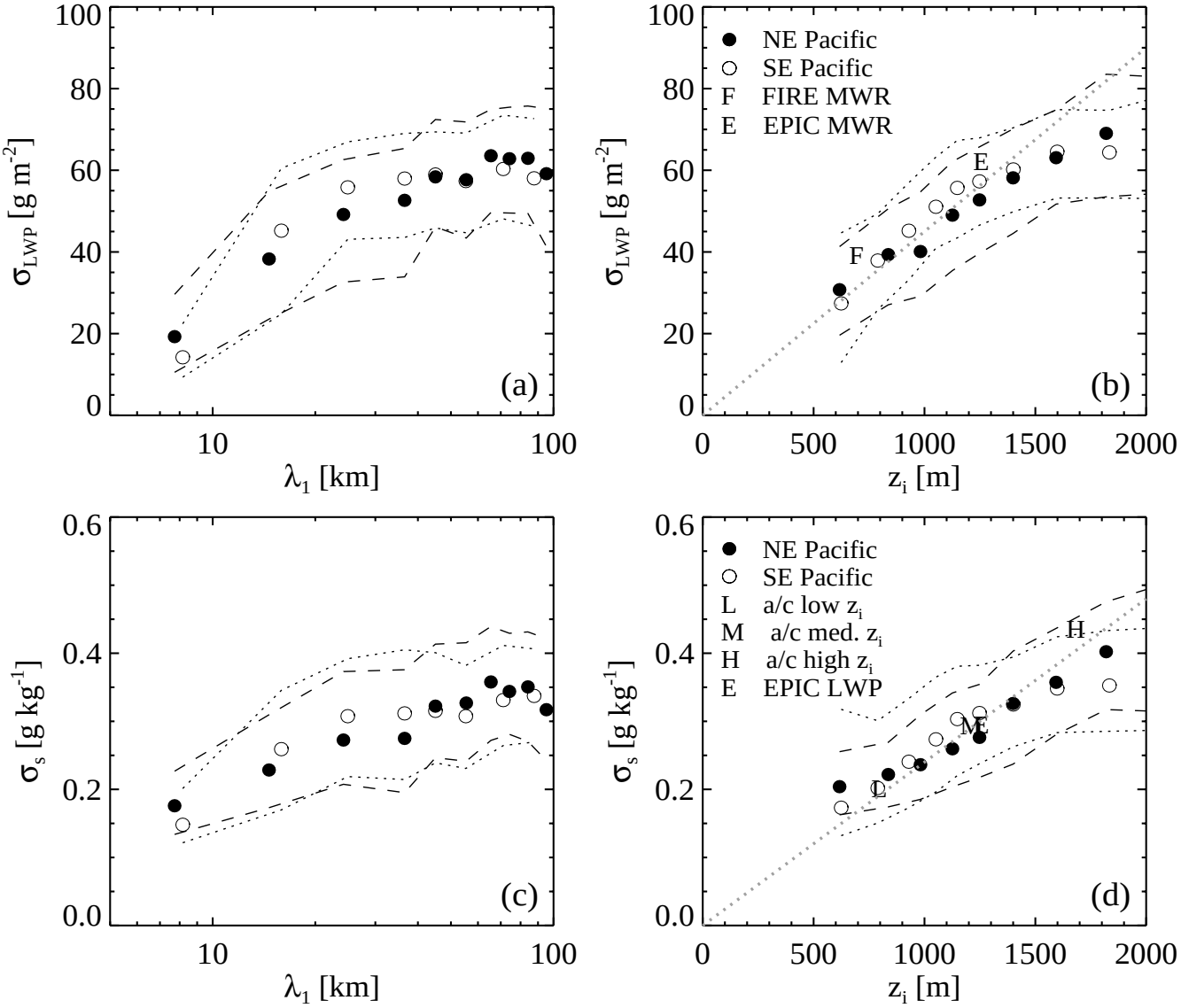
(a)
(b)
(c)
(d)
NE Pacific
SE Pacific
F FIRE MWR
E EPIC MWR
L a/c low z_i
M a/c med. z_i
H a/c high z_i
E EPIC LWP
σ_{LWP} [g m^{-2}]
σ_s [g kg^{-1}]
λ_1 [km]
z_i [m]

Figure 16:

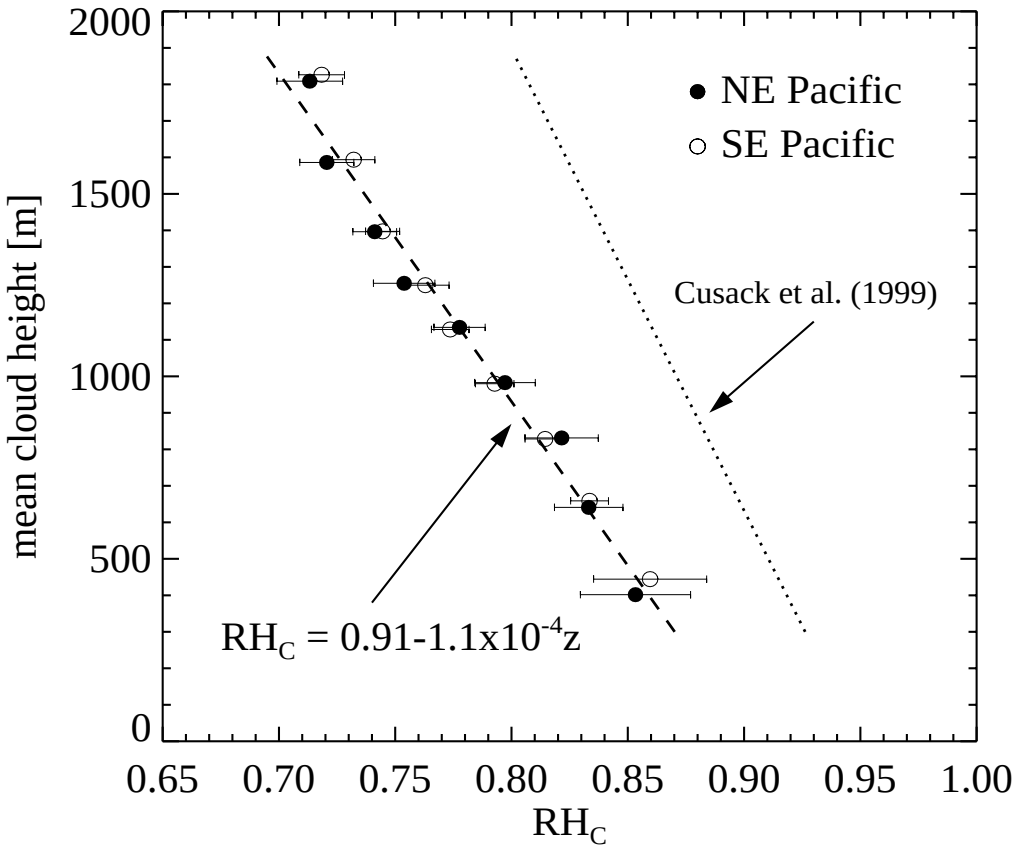
2000
1500
1000
500
0
mean cloud height [m]
0.65
0.70
0.75
0.80
0.85
0.90
0.95
1.00
RH$_C$
NE Pacific
SE Pacific
Cusack et al. (1999)
RH$_C$ = 0.91-1.1x10^{-4}z

Figure 17:

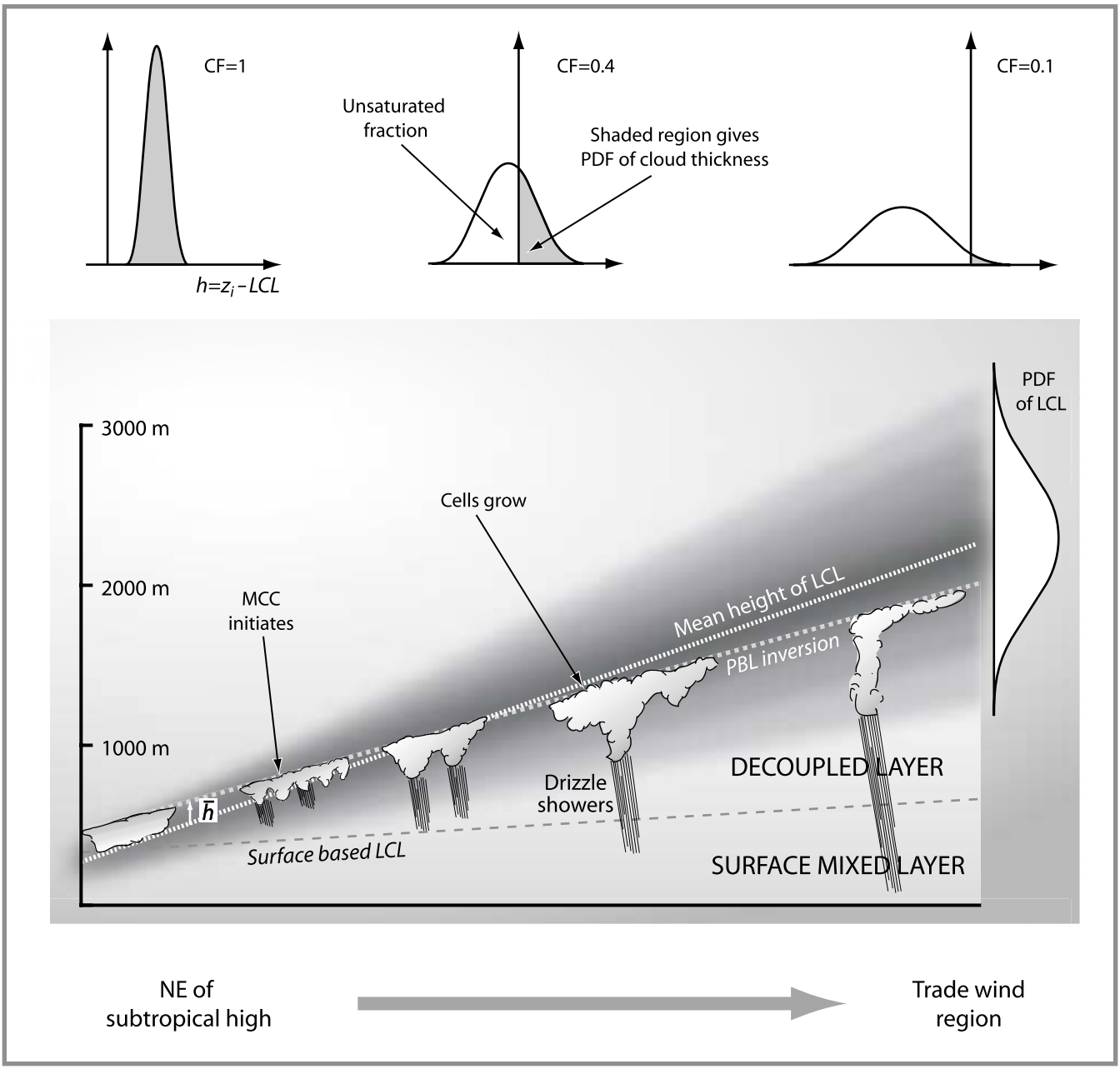
CF=1
CF=0.4
CF=0.1
Unsaturated fraction
Shaded region gives PDF of cloud thickness
h=z_i – LCL
PDF of LCL
3000 m
2000 m
1000 m
Cells grow
MCC initiates
Mean height of LCL
PBL inversion
DECOUPLED LAYER
Drizzle showers
h̄
Surface based LCL
SURFACE MIXED LAYER
NE of subtropical high
Trade wind region

Figure 18: